

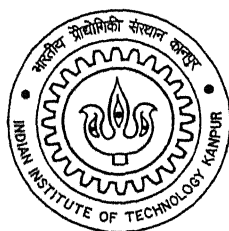
# Synthesis and Characterization of $\text{Li}_2\text{SO}_4$ -based glassy Superionic Conductors

A Thesis Submitted  
in Partial Fulfilment of the Requirements  
for the Degree of

**Master of Technology**

by

**Debasis Basu**



to the

**Department of Materials Science  
Indian Institute of Technology Kanpur**

**December, 2000**

590

/ms

133679

TH

MC/2000/rt

E-2792



133679

TH

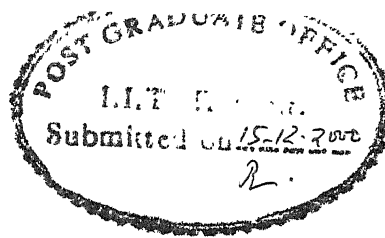
Mr 12000/11

E 2.792




A133679

# Certificate



It is certified that the work presented in this thesis entitled 'Synthesis and Characterization of  $\text{Li}_2\text{SO}_4$ -based glassy Superionic Conductors', by Debasis Basu, has been carried out under my supervision and that this work has not been submitted elsewhere for a degree.

IIT Kanpur  
December, 2000

  
(Prof. K. Shahi)  
Thesis Supervisor  
Materials Science Program  
IIT Kanpur

## **ABSTRACT**

The dc electrical conductivity of  $(\text{B}_2\text{O}_3 - 75 \text{ m/o Li}_2\text{O}) : x \text{ Li}_2\text{SO}_4$  glass system has been studied in the temperature range 400 to 500 K. The conventional quenching technique, two flat copper plates frozen at liquid nitrogen (77 K), has been used to form glass. To understand the enhancement in the electrical conductivity of the glass system and the effect of addition of  $\text{Li}_2\text{SO}_4$  both pure  $\text{Li}_2\text{SO}_4$  salt and the host system  $(\text{B}_2\text{O}_3 - 75 \text{ m/o Li}_2\text{O})$  have been studied first. The results have been explained on the basis of concentration of  $\text{Li}_2\text{SO}_4$  ( $x = 50, 40, 30, 20, 10 \text{ m/o}$ ) and  $\text{Li}^+$  ion fraction. The maximum enhancement in the conductivity is by two orders of magnitude with activation energy as low as 0.60 eV due to incorporation of 20 m/o  $\text{Li}_2\text{SO}_4$ . The glassy state in this series is quite stable with high transition temperatures varying from 476 to 608 K. Also the dielectric properties of the system have been investigated by studying the frequency dependence of impedance. It has been found that the dielectric constant varies from  $10^6$  to  $10^2$  for low ( $\sim 10\text{Hz}$ ) and high frequencies (10MHz) respectively. The dielectric constant is also quite sensitive to temperature as it changes by more than two orders of magnitude at lower frequencies. Like dielectric constant, the dielectric loss is also a strong function of frequency. But unlike dielectric constant its variation with temperature is much significant for a wide range of frequencies ( $\sim 10^2 \text{ Hz}$  to  $10^2 \text{ kHz}$ ).

# Acknowledgement

It is difficult to find any word to thank my thesis supervisor, Professor K Shahi for his valuable discussions and suggestions from my very first day at IIT Kanpur. It is his constant encouragement and enthusiasm which made this work possible.

I would like to thank all my friends- particularly Subrata, Sanjib, Ashish, Siddhartha, Sushovan, Jayram, Murali, Prabhakar, Shekhar for their warm and lovable association.

I am really grateful to my labmates Anshuman, Ramanujam, Krishna, Jai Prakash, Feroz, Ashotosh, Sudha for their spontaneous help and encouragement.

Also I am thankful to the Materials Science staffs Mr. B Sharma, Mr. Thapa, Mr. Pandey and Mr. Chaturi Singh, Mr. Umashankar.

# Contents

<b>1</b>	<b>Introduction</b>	<b>1</b>
1.1	Superionic Conductors . . . . .	1
1.2	Trends in SICs . . . . .	2
1.2.1	Composites: . . . . .	2
1.2.2	Mixed Crystals: . . . . .	2
1.2.3	Polymers: . . . . .	3
1.2.4	Glassy Superionics: . . . . .	3
1.3	The Present Investigation . . . . .	3
1.3.1	B <sub>2</sub> O <sub>3</sub> as Glass Network Former: . . . . .	4
1.3.2	Glass Modifier: . . . . .	5
1.3.3	Incorporation of Mobile Ion: . . . . .	7
1.3.4	The <i>Host</i> System: B <sub>2</sub> O <sub>3</sub> -Li <sub>2</sub> O: . . . . .	7
1.3.5	Li <sub>2</sub> SO <sub>4</sub> as the Dopant Salt: . . . . .	11
1.3.6	The System (B <sub>2</sub> O <sub>3</sub> :75 m/o Li <sub>2</sub> O):xLi <sub>2</sub> SO <sub>4</sub> : . . . . .	12
1.4	General Theory of Ionic Conduction: . . . . .	13
<b>2</b>	<b>Characterization Techniques &amp; Experimental Details</b>	<b>15</b>

2.1	<b>Structural Analysis</b>	15
2.2	<b>Impedance Analysis</b>	16
2.2.1	Purely Resistive:	18
2.2.2	Purely Capacitive:	18
2.2.3	Series Combination of R and C:	19
2.2.4	Parallel Combination of R and C:	20
2.3	<b>Experimental Setup</b>	25
2.3.1	Sample Holder:	26
2.3.2	Furnace and Temperature Controller:	26
2.3.3	Impedance Analyzer:	29
2.4	<b>Materials Processing</b>	30
2.4.1	Synthesis of Glasses:	30
2.4.2	Pelletization and Electrodes:	31
2.5	<b>Impedance Measurement</b>	33
3	<b>Results &amp; Discussion</b>	35
3.1	<b>X-ray Diffraction:</b>	35
3.2	<b>Impedance Analysis</b>	40
3.2.1	DC Conductivity:	43
3.3	<b>Electrical Conductivity Vs. Temperature</b>	45
3.3.1	Pure $\text{Li}_2\text{SO}_4$	45
3.3.2	The Host System	47
3.3.3	Glasses	49
3.4	<b>Electrical Conductivity Vs. Composition:</b>	54
3.4.1	Transition Temperature	60
3.5	<b>Impedance Vs. Frequency</b>	63



CONTENTS	ix
3.5.1 Dielectric Constant and Loss . . . . .	68
3.5.2 Activation Energy Revisited . . . . .	70
4 Conclusion	72

## Figure Caption

1.1	Structure of boron-oxygen network in (a)crystalline and (b) glassy materials	5
1.2	Schematic two-dimensional representation of complex oxygen-borate network with lithium oxide as glass structure	6
1.3	The structural groups observed in the borate systems	8
2.1(a)	Impedance plot for a purely resistive circuit	18
2.1(b)	Impedance plot for a purely capacitive circuit	19
2.1(c)	Impedance plot for a resistor and a capacitor in series	20
2.1(d)	Impedance plot for a resistor and a capacitor in parallel	22
2.2(a)	Effect of interface capacitance on impedance of electrolyte	22
2.2(b)	Depression of semicircle due to multipole polarization	23
2.2(c)	Grain boundary effect	24
2.3	Block diagram of the experimental set-up used in the ionic conductivity measurement	25
2.4	Sample holder for impedance measurement	27
3.1(a)	XRD pattern for the crystalline mixture and quenched material for S50 sample	36
3.1(b)	XRD pattern for the crystalline mixture and quenched material for S30 sample	38
3.1(c)	XRD pattern for the crystalline mixture and quenched material for S20 sample and quenched host system	39

3.2	Impedance plots for pure $\text{Li}_2\text{SO}_4$ at various temperature	40
3.3	Impedance plot for 20 mol% $\text{Li}_2\text{SO}_4$ glass composition	42
3.4	Logarithm of ac conductivity vs inverse temperature plot for pure $\text{Li}_2\text{SO}_4$ at frequencies 5 and 10 kHz	44
3.5	Logarithm of dc conductivity vs inverse temperature plot for pure $\text{Li}_2\text{SO}_4$	46
3.6	Logarithm of dc conductivity vs. inverse temperature plot for host system [ $\text{Li}_2\text{O} + 25\% \text{B}_2\text{O}_3$ ]	48
3.7	Logarithm of dc conductivity vs. inverse temperature plot for 10 mol% $\text{Li}_2\text{SO}_4$ glass (sample S10)	49
3.8	Logarithm of dc conductivity vs. inverse temperature plot for 20 mol% $\text{Li}_2\text{SO}_4$ glass (sample S20)	50
3.9	Logarithm of dc conductivity vs. inverse temperature plot for both heating and cooling cycles in the glassy state for S20 sample	52
3.10	A comparison of electrical conductivity of the S20 glass (in cooling cycle) with that of crystalline mixture of the same composition	53
3.11	Dissociation mechanism of $\text{Li}_2\text{SO}_4$ in the LB system	54
3.12	The variation of electrical conductivity as a function of inverse temperature for six different compositions	56
3.13	Variation of electrical conductivity with composition at $T = 400$ and $500 \text{ K}$	57
3.14	Variation of activation energy $E_a$ with composition	59
3.15	Variation of transition temperature $T_g$ with composition	61

3.16 Frequency dependence of the imaginary part $Z''$ of the complex impedance at various temperature for S20 glass	64
3.17a The relaxation frequency $\omega_r$ vs inverse of temperature plots from $Z''$ calculation for sample S20	66
3.17b The FWHM $\Delta\omega$ vs inverse of temperature plots from $Z''$ calculation for sample S20	66
3.18 The dielectric constant as a function of frequency for the glass S20 at different temperatures	67
3.19 Dielectric loss ( $\tan\delta = \epsilon''/\epsilon'$ ) vs. frequency plot for S20 glass	68
3.20a $\text{Log}(\omega_r/2\pi)$ vs. $10^3/T$ plots obtained from dielectric loss for $x = 20$ composition	70
3.20b $\text{Log}(\Delta\omega/2\pi)$ vs. $10^3/T$ plots obtained from dielectric loss for $x = 20$ composition	70

## **List of Tables**

1.1	Examples of Composites	2
1.2	Examples of mixed crystals	2
1.3	Conductivities of $B_2O_3$ - $Li_2O$ for different Compositions	9
2.1	The displays of the Analyzer	28
2.2	The physical and chemical properties of starting materials	29
2.3	The compositions of the samples investigated	30
3.1	Characteristic features of pure $Li_2SO_4$	47
3.2	Transition temperature, conductivity and activation energy values for different compositions	62
3.3	The values of relaxation frequency, FWHM extracted from various processes	69
3.4	Activation energy values extracted from various processes	71

# Chapter 1

## Introduction

### 1.1 Superionic Conductors

A particular class of ionic solids so called superionic or fast ionic conductors (SIC/FIC), have more vacant sites than ions to fill them, only a modest barrier between nearly equivalent sites and connected path ways through the bulk. With these characteristics, such materials exhibit high ionic conductivity ( $\sim 1\Omega^{-1}\text{cm}^{-1}$ ) even at lower temperatures, well below their melting points. SICs are electronically insulators with high band gap.

The SICs have attracted considerable attention in recent years mainly because their potential applications in the fields of electrochemical cells, power sources, oxygen concentration cells, fuel cells, thermoelectric power generator etc.<sup>[1,2]</sup> Moreover, many of the SICs undergo a first order transition accomplished by exciting changes in their physical properties such as electrical conductivity, thermopower, specific heat etc.

## 1.2 Trends in SICs

### 1.2.1 Composites:

Enhancement of ionic conductivity is possible by dispersion of fine particles of a chemically inert and electrically neutral material in the ionic solid. A highly conducting layer is developed surrounding the particles of dispersoid. A few examples are listed in the Table 1.1.

**Table 1.1:** Examples of composites:

Ionic solid	Dispersoid	Enhancement factor
PbI <sub>2</sub>	Al <sub>2</sub> O <sub>3</sub>	30
AgI	SiO <sub>2</sub>	45
AgI	Fly ash	51
CsCl	Al <sub>2</sub> O <sub>3</sub>	708
AgI	Al <sub>2</sub> O <sub>3</sub>	2500

### 1.2.2 Mixed Crystals:

Ionic crystals can dissolve relatively large amounts of homovalent ions (e.g., AgI:Br<sup>-</sup>) with homovalent ions and owing to lattice distortion, they exhibit high ionic conductivity. Such systems are referred to as mixed crystals or solid solutions.

**Table 1.2:** Examples of mixed crystals:

Host ionic solid	Dopant ion	Enhancement factor
AgBr	I <sup>-</sup>	77
AgI	Br <sup>-</sup>	1000

### 1.2.3 Polymers:

Electrolytes obtained from polymers play an important role in the applications of storage cell. The advantages with the polymers are due to their light weight, elasticity, flexibility etc.

Example: PEG (LiClO<sub>4</sub>)(Al<sub>2</sub>O<sub>3</sub>).

### 1.2.4 Glassy Superionics:

Glasses are inherently disordered materials and possess relatively high conductivity. Thus, in recent years, considerable effort has been made to develop highly conducting glassy materials. The aim of the present work was to synthesize Li<sup>+</sup>-based glassy superionic conductors suitable for battery and other electrochemical devices.

## 1.3 The Present Investigation

The glassy solid electrolytes have become the focus of interest in the recent past due to several advantages over their crystalline counterparts.<sup>[3,4]</sup> For the crystalline materials, further improvement gets restricted because of their certain limitations. Firstly, the structural arrangement allows the motion of ions only along crystallographic axes. Secondly, only a few crystalline materials, termed as “optimum materials”, are found to have high density of weakly bonded ionic species. Moreover, for most technological applications, single crystals are not very practical and in case of polycrystalline ceramics, discontinuity of mobile ion channels are found at the grain boundaries.

The above mentioned problems are not present in the glasses. For instance, (i) the long range translational symmetry of the crystalline structure is lacking in glass-



es, (ii) the structural requirements are not so severe because of high degree of disorder, (iii) the conductivity is same in all directions as it is isotropic, (iv) in glasses, without being restricted to one particular system, one can obtain many systems by changing the composition continuously of the constituents such as glass network former, glass modifier and the mobile ion incorporating ionic compound over a wide range. Besides, from the practical applications point of view, (v) it is easy to form thin films from glass<sup>[5]</sup> and (vi) flexibility of size and shape is there<sup>[6]</sup> at satisfactory cost. (vii) Also in the glassy systems, the ionic conductivity avoids the problem associated with grain boundaries.

In addition to that (viii) glasses have good redox stability. (ix) Due to potential fluctuations imposed by disordered structure, the coherence length of electrons get shortened and thus their mobility becomes weak.<sup>[7]</sup> So, the electronic contribution to the conductivity is much less than that due to ions, which is an important condition for a candidate to be considered as a good electrolyte. (x) Near the glass transition temperature  $T_g$ , a material becomes very soft, so extremely good contact<sup>[5]</sup> is made between the electrodes and electrolyte. In fact this is especially a critical condition for interaction-type electrodes whose volume vary during the charge-discharge cycles. Depending upon the requirements,  $T_g$  can be changed by controlling the heating or cooling rate.

### 1.3.1 B<sub>2</sub>O<sub>3</sub> as Glass Network Former:

The well-known and frequently used glass formers are B<sub>2</sub>O<sub>3</sub>, P<sub>2</sub>O<sub>5</sub>, GeO<sub>2</sub>, SiO<sub>2</sub>, Al<sub>2</sub>O<sub>3</sub> etc. The most important feature for which the glasses are being used as solid electrolyte, is their disordered structure. They consist of elementary units such as triangles, tetrahedra etc. In their crystalline state these units are present but in a well-ordered fashion. Only in their glassy state, the valence angles and bond lengths of the units are dispersed,<sup>[8]</sup> and they are randomly oriented in 3-D (as shown in Fig.1.1).

In order to obtain glassy state, the appropriate mixture is melted first and then the melt is rapidly cooled (quenched) using different techniques. Keeping in mind, the fact that for development of a glass with a lower  $T_g$  and the availability of the kanthal wire wound furnaces which can go only upto  $1100^\circ\text{C}$ ,  $\text{B}_2\text{O}_3$  may be considered to be a good choice as a glass network former due to its lower melting point ( $T_M=450^\circ\text{C}$ ) than others such as  $\text{P}_2\text{O}_5$  ( $580^\circ\text{C}$ ),  $\text{GeO}_2$  ( $1115^\circ\text{C}$ ),  $\text{SiO}_2$  ( $1723^\circ\text{C}$ ) and  $\text{Al}_2\text{O}_3$  ( $2072^\circ\text{C}$ ).

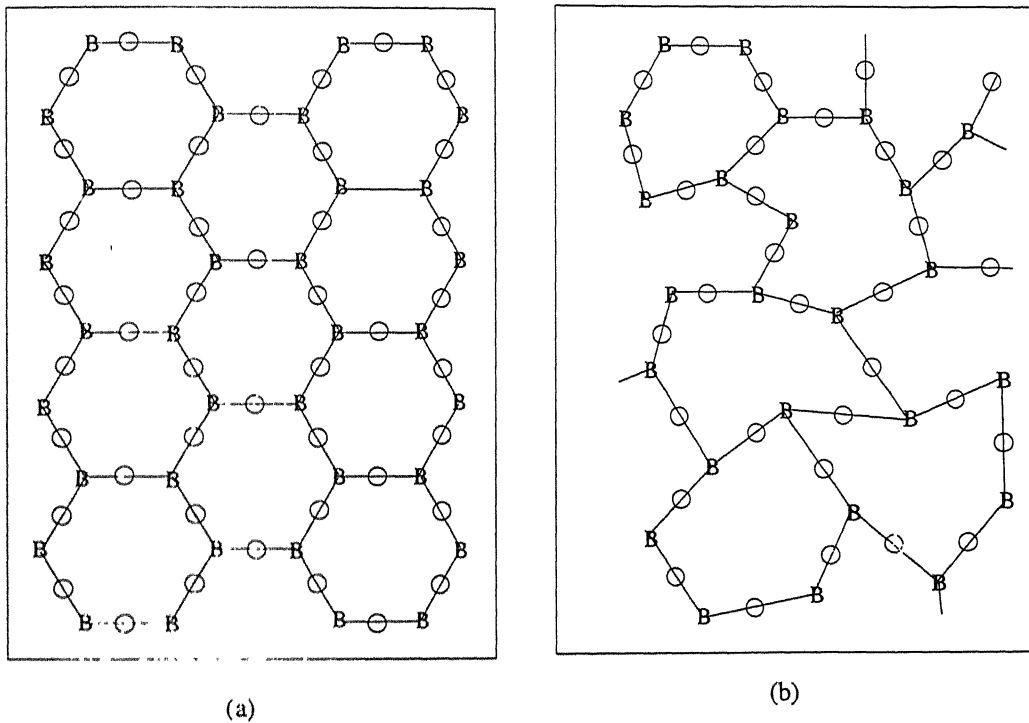


Fig.1.1: Structure of boron-oxygen network in (a) crystalline and (b) glassy materials. Here B and O represent boron and oxygen atoms respectively.

### 1.3.2 Glass Modifier:

The glassy arrangement is further broken by glass modifier. The oxides, chalcogenides of alkali, alkaline earth or silver cations do influence the structural changes

in the networks of the glass formers. They are thus called glass modifiers. The modifiers introduce ionic bonds between the modifier cations and the covalent chains in the glass matrix. The positively charged interstitial cations are accommodated by inclusion of the modifier anions into the chains. If the modifier concentration is increased, the distance between two adjacent negative anion sites decreases. When such widely spaced anions are highly interconnected, favorable channels for transport of mobile ions are formed. Hence, ionic conductivity increases with insertion of glass modifiers.

In the case of oxide glasses, the modifier cations widens the space in the glass matrix by producing non-bridging oxygens (NBO) by breaking the oxygen bonds. In Fig.1.2 the structure of borate glass in presence of  $\text{Li}_2\text{O}$  as alkali modifier has been shown. Non-bridging oxygen atoms are found in the Fig.1.2 as dangling open bonds.

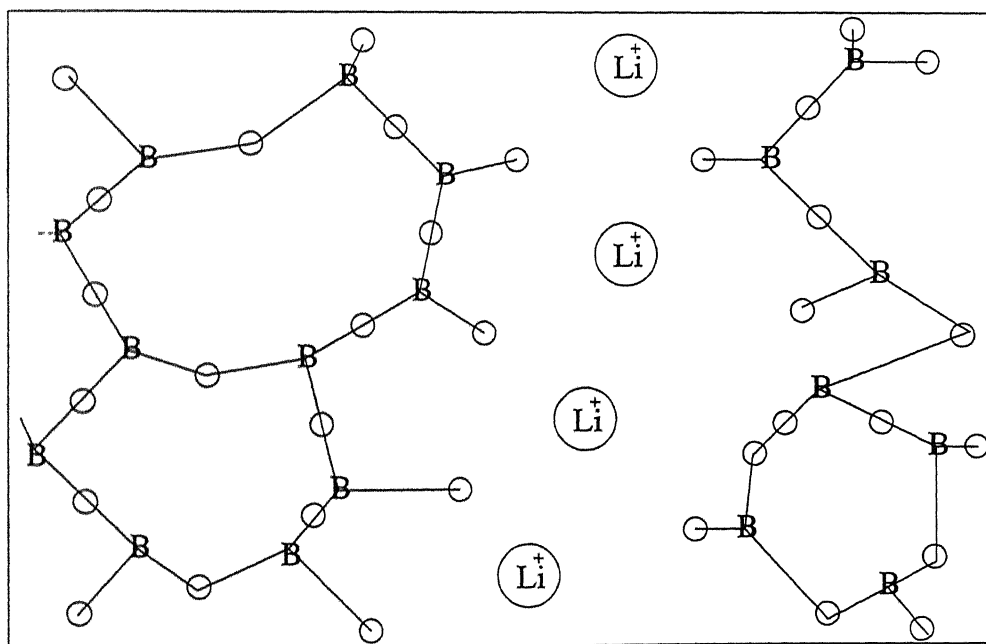


Fig.1.2: Schematic two-dimensional representation of complex oxygen-borate network with lithium oxide as glass structure. Here B, O and  $\text{Li}^+$  represent boron, oxygen and lithium respectively.

### 1.3.3 Incorporation of Mobile Ion:

An ionic salt is introduced into the glass matrix to incorporate mobile ions. Generally, the halogens, sulphates or phosphates of the same cation as that of the network modifier is chosen as dopant salt to incorporate only one type of cation as charge carrier. In that case, it has been found that both cations and anions are accommodated into the glass matrix and cation interstitials carry the electricity.

Lithium ion conducting glasses offer better prospects in high energy density storage cells and other electrochemical applications than others, because lithium has (i) lower equivalent weight, and (ii) is most electropositive element<sup>[9]</sup> These two features combine to yield a very high energy density for Li-batteries. In addition, in case of  $\text{Li}^+$  ion conducting systems, several cathode materials can be employed as they offer high Li-diffusion coefficient.<sup>[2,3,5]</sup>

### 1.3.4 The *Host* System: $\text{B}_2\text{O}_3\text{-Li}_2\text{O}$ :

According to Krogh-Moe,<sup>[10]</sup> the structure of a pure  $\text{B}_2\text{O}_3$  consists of a network of boroxol rings and  $\text{BO}_3$  triangles connected by B-O-B linkage with bridging oxygens. The addition of alkali oxides modifies the boroxol rings and complex diborate and tetraborate groups are formed and they are found to be randomly oriented.<sup>[11]</sup> These  $\text{BO}_4$ -tetrahedra finally get converted into pyroborate and orthoborate. This pyro- and orthoborate groups contain non bridging oxygen (NBO) as shown in Fig.1.3. In this way, alkali ions break the oxygen bonds and form non bridging oxygens (NBOs).

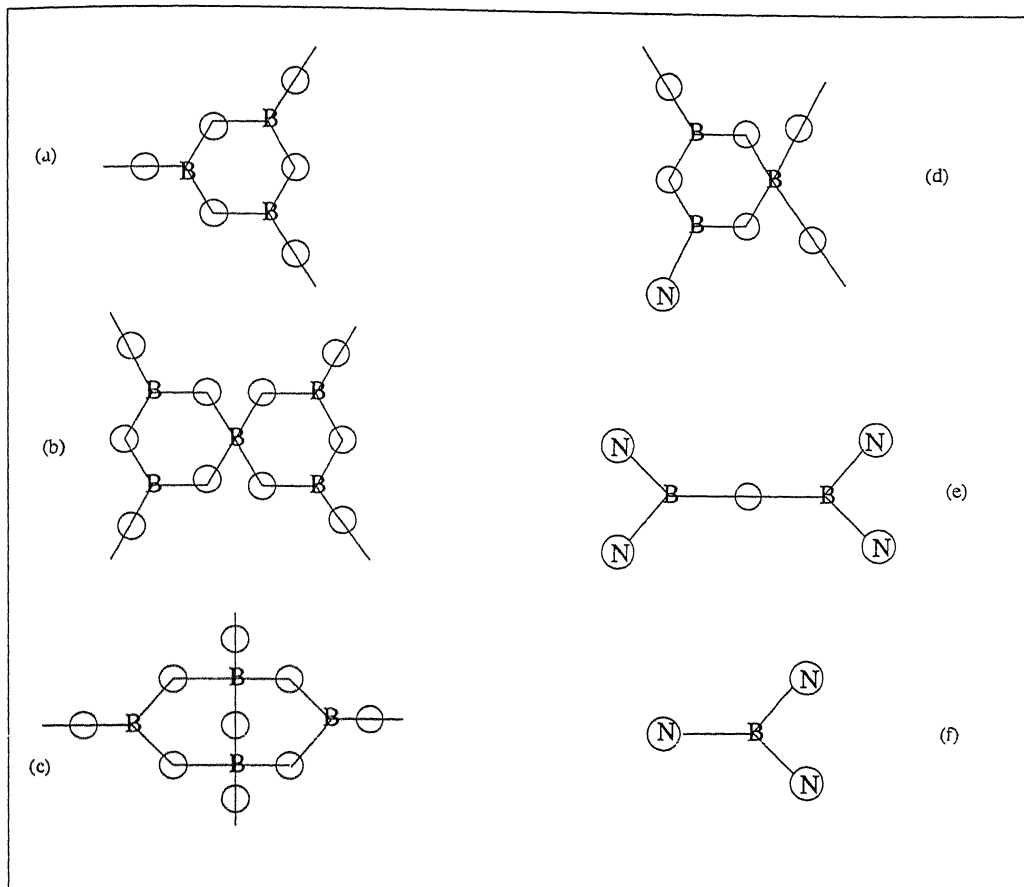


Fig.1.3 : The structural groups observed in borate systems. B, O, N stand for boron, bridging oxygen and non-bridging oxygen atoms. The groups are: (a) boroxol ring, (b) tetraborate, (c) diborate, (d) triborate with one NBO, (e) pyroborate and (f) orthoborate.

The existing holes with bridging oxygen yield high energy sites for the mobile ions. However, these NBOs act as low energy trapping sites,<sup>[7]</sup> which are thus favorable to ionic conduction. Lithium oxide has been chosen as glass modifier. The available conductivity values of some compositions of  $B_2O_3$ - $Li_2O$  system have been listed in Table 1.3.

**Table 1.3: Conductivities of B<sub>2</sub>O<sub>3</sub>-Li<sub>2</sub>O for different compositions:**

Composition B <sub>2</sub> O <sub>3</sub> :Li <sub>2</sub> O	Conductivity $\sigma$ ( $\Omega^{-1}\text{cm}^{-1}$ )	Temperature T (K)	Activation energy $E_a$ (eV)	Reference
95 : 5	$<5.68 \times 10^{-9}$	623	-	14
90 : 10	$<1.78 \times 10^{-9}$	623	-	14
85 : 15	$<3.85 \times 10^{-9}$	623	-	14
79.5 : 20.5	$1.31 \times 10^{-7}$	623	-	14
75 : 25	$4.07 \times 10^{-5}$	623	-	14
60 : 40	$4.02 \times 10^{-5}$	625	0.99	5
60 : 40	$4.70 \times 10^{-6}$	473	-	5
57.5 : 42.5	$6.13 \times 10^{-3}$	623	0.60	14
57.5 : 42.5	$2.54 \times 10^{-3}$	623	0.75	15
57 : 43	$2.98 \times 10^{-3}$	473	0.66	13
50 : 50	$5.30 \times 10^{-6}$	473	-	15
43 : 57	$6.30 \times 10^{-11}$	298	0.73	7
40 : 60	$4.00 \times 10^{-4}$	473	-	15

The B<sub>2</sub>O<sub>3</sub>-Li<sub>2</sub>O system has been extensively studied over the last two decades. In all most all cases, the LB systems with less Li<sub>2</sub>O content have been chosen. However, this approach has changed in recent years. Much stress is being given to systems with high Li<sub>2</sub>O content. The present view is that Li<sub>2</sub>O takes part in modifying the network as well as incorporating Li<sup>+</sup> ions to the matrix.<sup>[12]</sup> So high Li<sub>2</sub>O content glasses can offer materials with high ionic conductivity.

On the contrary, there are problems with glasses containing lesser Li<sub>2</sub>O and higher B<sub>2</sub>O<sub>3</sub>. It has been found that some particular compositions with high B<sub>2</sub>O<sub>3</sub> content cause two phase liquid system when heated above the melting point of the

material. This finally results in no glass formation at all.<sup>[13]</sup>

High  $\text{Li}_2\text{O}$  content glasses have the following advantages:

1. The network forming ability is associated with four-fold coordination of cation (Lithium) by oxygen ions, i.e.,  $\text{LiO}_4$ -tetrahedra.<sup>[12]</sup> A considerable number of  $\text{LiO}_4$  would be expected for glasses with more than 50 m/o  $\text{Li}_2\text{O}$ .
2.  $\text{Li}^+$  ions attached to  $\text{BO}_4$  are more mobile. Therefore larger number of  $\text{BO}_4$  is expected rather than  $\text{BO}_3$ . For high  $\text{Li}_2\text{O}$  content systems progressive  $\text{BO}_4$ -tetrahedra formation is possible.<sup>[11,16]</sup>
3. Participation of Lithium in network has also been postulated for very large ratio of  $\text{Li}_2\text{O}$ .<sup>[12]</sup>
4. Around 65 m/o  $\text{Li}_2\text{O}$  gives the peak in the continuous glass forming region.<sup>[12]</sup>
5. High  $\text{Li}_2\text{O}$  ( $\geq 70$  m/o) slows down the crystallization process, i.e., offers better quality glasses.<sup>[17]</sup>
6. More  $\text{Li}_2\text{O}$  ( $\geq 50$  m/o) results in larger number of non-bridging oxygens (N-BOs) in the system.<sup>[8]</sup> These NBOs play an important role in forming wide channels.
7.  $\text{B}_2\text{O}_3$  needs less activation energies above 45 m/o  $\text{Li}_2\text{O}$ .
8.  $T_g$  decreases with increase in  $\text{Li}_2\text{O}$  fraction above 25 m/o.<sup>[18]</sup>
9. With  $\text{Li}_2\text{O}$ , mobile  $\text{Li}^+$  ions increase. So conductivity gets enhanced as ionic charge density increases.

In early days, researchers restricted the  $\text{Li}_2\text{O}$  concentration to less than 45 m/o, to ensure the formation of glass. But this view changed of late.<sup>[19]</sup> The glassy state conductivity is lower than their nearest oxide glass equivalent<sup>[13]</sup> (i.e., glass forming

alkali salts). With this consideration, maximum conductivity can be achieved by increasing salt-like character at lowest  $B_2O_3$  contents. At a molecular level,  $Li_2O$  amount can be increased to make the saturation of the alkali salt in the glass. In other words, to increase  $Li_2O$  means increase in packing efficiency and thus approaching towards the “ideal glass” condition.

Also it is appreciated that the glass forming region of LB glasses can be extended by a faster quenching technique.<sup>[20]</sup> With the availability of faster quenching processes, the more recent trend is to work with higher ratio of  $Li_2O$ . E I Kamitsos *et al* have studied a system with 71 m/o  $Li_2O$ .<sup>[21]</sup> In the present study,  $B_2O_3$ :75 m/o  $Li_2O$  has been chosen as the host system.

### 1.3.5 $Li_2SO_4$ as the Dopant Salt:

The importance of Lithium batteries and hence  $Li^+$ -ion based solid electrolytes has already been discussed. With that logic,  $Li_2O$  has already been selected as the glass modifier. It has also been mentioned that the same cation is generally taken as the modifier as well as the dopant salt. The available choices for the dopant salt are  $Li_nX$  [ $X = F, Cl, Br, I, SO_4$  etc.]. However,  $Li_2SO_4$  was as chosen dopant salt for this study mainly because it is a well known superionic conductor at high temperatures ( $T \geq 575\text{ }^\circ C$ ) and it was anticipated that the high temperature superionic phase may get stabilized at lower temperatures. Besides, another requirement for glass formation is that the anion  $X^{n-}$  should dissolve into the glass matrix. It has been reported that larger the anion size, higher is the tendency of the salt to dissociate.<sup>[15]</sup> Sulphate ion is large in size. Therefore one can expect that  $SO_4^{2-}$  ion will get dissolved easily. With that expectation  $Li_2SO_4$  has been chosen as the dopant salt.



### 1.3.6 The System (B<sub>2</sub>O<sub>3</sub>:75 m/o Li<sub>2</sub>O):xLi<sub>2</sub>SO<sub>4</sub>:

The fraction of the glass modifier added to the glass former is an important factor in determining the structure of the glass.<sup>[21]</sup> Because the relative number of the tetrahedra and triangles i.e., 3- and 4-coordinated boron as well as the types of groups present in the matrix strongly depends upon this ratio. Therefore keeping B<sub>2</sub>O<sub>3</sub> and Li<sub>2</sub>O ratio fixed as 1:3 (B<sub>2</sub>O<sub>3</sub>:75 m/o Li<sub>2</sub>O), the fraction of Li<sub>2</sub>SO<sub>4</sub> can be varied systematically to understand the effect of the same on the host system. It has been found that the addition of Li<sub>2</sub>SO<sub>4</sub> does not affect the glass network fundamentally, even when added with high concentrations<sup>[17]</sup> No appreciable reaction has been noticed between the boron-oxygen network and the Li<sub>2</sub>SO<sub>4</sub>.<sup>[22]</sup> For that reason the ternary system can be considered as the solution where the glass former B<sub>2</sub>O<sub>3</sub> and the glass modifier Li<sub>2</sub>O constitute the solvent while the dopant salt Li<sub>2</sub>SO<sub>4</sub> is the solute.

## 1.4 General Theory of Ionic Conduction

The conductivity of a normal ionic solid such as alkali halides which exhibit Schottky disorder is given by

$$\sigma = \sigma_c + \sigma_a \quad (1.1)$$

$$= n_c(T)q\mu_c(T) + n_a(T)\mu_a(T) \quad (1.2)$$

where  $\sigma$  is the conductivity,  $n$  the density,  $\mu$  the mobility and  $q$  the charge of the mobile defects per particle,  $T$  the temperature, and the subscripts  $c$  and  $a$  denote the cation and anion vacancies respectively.

The temperature dependent terms like  $n(T)$  and  $\mu(T)$  are given by

$$n = B \exp\left(-\frac{g_F}{2KT}\right) \quad (1.3)$$

$$\mu = \frac{\mu_o}{T} \exp\left(-\frac{g_m}{KT}\right) \quad (1.4)$$

Assuming that only one type of mobile species makes a significant contribution to the observed conductivity, Eq. 1.2 becomes

$$\sigma T = A \exp\left(-\frac{\left(\frac{g_F}{2} + g_m\right)}{KT}\right) \quad (1.5)$$

$$\Rightarrow \ln \sigma T = \ln A - \frac{1}{KT} \left(\frac{g_F}{2} + g_m\right) \quad (1.6)$$

$$\Rightarrow \ln \sigma T = \ln A - \frac{E_a}{KT} \quad (1.7)$$

with

$$E_a = \left(\frac{g_F}{2} + g_m\right) \quad (1.8)$$

where,  $E_a$  = activation energy,  $g_m$  = migration energy,  $g_F$  = formation energy and  $K$  = Boltzmann constant.

The variation of  $\ln T$  over the experimental temperature region (300K to 800K) is negligible in comparison to that of  $\ln \sigma$ . Therefore Eq.1.7 can be written as

$$\ln \sigma = \ln A - \frac{E_a}{KT} \quad (1.9)$$

For the low temp. region, the energy is due to the migration only,

$$\ln \sigma = \ln A' - \frac{g_m}{T} \quad (1.10)$$

Here the curves are drawn for  $\ln \sigma$  vs.  $\frac{10^3}{T}$ , so equation (10) becomes

$$\ln \sigma = \ln A - \frac{E_a}{10^3 K} \cdot \left(\frac{10^3}{T}\right) \quad (1.11)$$

and eqn. (11) becomes

$$\ln \sigma = \ln A' - \frac{g_m}{10^3 K} \cdot \left(\frac{10^3}{T}\right) \quad (1.12)$$

Equations 1.12 and 1.13 are equations of straight line whose slopes are used to determine  $E_a$  and  $g_m$ . Formation energy can be calculated from the values of activation energy ( $E_a$ ) and migration energy ( $g_m$ ) by using eq. 1.18.

Above consideration is valid for crystalline materials, in general. But in case of glasses, the energy is due to migration only, as the mobile ions are by default present there. Therefore the activation energy for the glasses can readily be calculated from eq. 1.11.

## Chapter 2

# Characterization Techniques & Experimental Details

### 2.1 Structural Analysis

As far as ionic conduction is concerned, the structure of the material under investigation is very important. In order to know the atomic arrangement, XRD analysis of the material is done. As we know, every element or compound produces its own characteristic XRD peaks from which its structure can be determined.

The present investigation deals with glassy ionic materials. The glasses do not possess long range order but consists of randomly oriented units such as  $\text{SiO}_4$ -tetrahedra, boroxol rings etc. in  $\text{SiO}_2$  and  $\text{B}_2\text{O}_3$  glasses respectively. For randomly oriented structures, no peaks are recorded in the XRD studies. Thus to determine whether a material is in glassy state, XRD analysis has been performed using Richeifort (Iso - Debyelex 200 2D) counter diffractometer employed with a filtered  $\text{CuK}\alpha$  radiation.

## 2.2 Impedance Analysis

Ionic conduction is an electro-chemical process. In such a process, dc measurements cannot be made to get dc conductance because of polarisation at the electrode-electrolyte interfaces. Therefore ac measurements are generally carried out in order to obtain complex impedance from which the dc conductivity is extracted

When an ac signal, preferably a sinusoidal one, given by

$$v(t) = V_o e^{j\omega t} \quad (2.1)$$

is applied to a solid electrolyte, the resulting current is given by

$$i(t) = I_o e^{j(\omega t + \theta)} \quad (2.2)$$

where  $V_o$  and  $I_o$  are amplitudes of the applied voltage and the resulting current respectively,  $\omega$  the frequency and  $\theta$  the phase shift.

Thus the complex impedance is given by

$$Z^* = Z e^{j\omega t} \quad (2.3)$$

$$= Z \cos\theta + j \sin\theta \quad (2.4)$$

$$= Z_R + j Z_I \quad (2.5)$$

$$(or Z^* = Z' + j Z'') \quad (2.6)$$

with

$$Z = (Z'^2 + Z''^2)^{1/2} \quad (2.7)$$

and

$$\tan\theta = \frac{Z''}{Z'} \quad (2.8)$$

Now the dielectric related terms can also be calculated from the same (measured) complex impedance data ( $Z$  and  $\theta$ ) using the relationships stated below. Dielectric constant or relative permittivity  $\epsilon^*$ , is given by

$$\epsilon^* = \epsilon' - j\epsilon'' \quad (2.9)$$

with

$$\epsilon' = \frac{\sin\theta}{\omega C_o Z} \quad (2.10)$$

$$(2.11)$$

$$\epsilon'' = \frac{\cos\theta}{\omega C_o Z} \quad (2.12)$$

Dielectric loss defined by

$$\tan\delta = \frac{\epsilon''}{\epsilon'} \quad (2.13)$$

can be written in terms of  $Z'$  and  $Z''$  as

$$\tan\delta = \frac{Z'}{Z''} \quad (2.14)$$

Experimentally we measure the impedance of a complex assembly containing the solid electrolyte, electrodes, electrical leads etc. To analyse the system, the complex assembly can be modeled in the following combinations of resistors and capacitors:

### 2.2.1 Purely Resistive:

A pure resistor with resistance  $R$  governs

$$Z' = R, \quad Z'' = 0. \quad (2.15)$$

For such a case, the impedance plot with  $Z'$  and  $Z''$  as real and imaginary axes respectively will be an invariant point at  $Z' = R$  (Fig. 2.1(a))

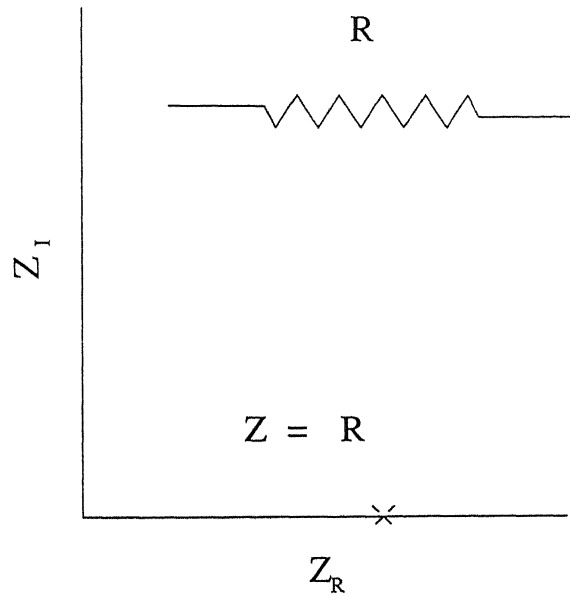


Fig. 2.1(a)

Fig. 2.1(a): Impedance plot for a purely resistive circuit

### 2.2.2 Purely Capacitive:

For a system with a pure capacitor of capacitance  $C$ , we get

$$Z' = 0, \quad Z'' = -\frac{1}{\omega C}. \quad (2.16)$$

The corresponding impedance plot will give a straight line parallel to the negative imaginary axis at  $Z' = 0$ .

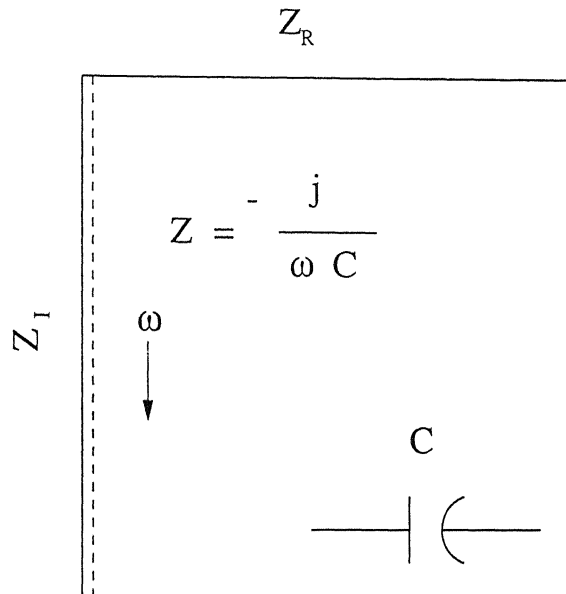


Fig. 2.1(b)

Fig. 2.1(b): Impedance plot for a purely capacitive circuit

### 2.2.3 Series Combination of R and C:

When the assembly behaves like a series combination of a resistor R and a capacitor C, one gets

$$Z^* = R - \frac{j}{\omega C}. \quad (2.17)$$



with

$$Z' = R \quad (2.18)$$

$$Z'' = -\frac{1}{\omega C}. \quad (2.19)$$

This essentially gives a straight line parallel to the negative imaginary axis at  $Z' = R$ , as shown in Fig. 2.1(c).

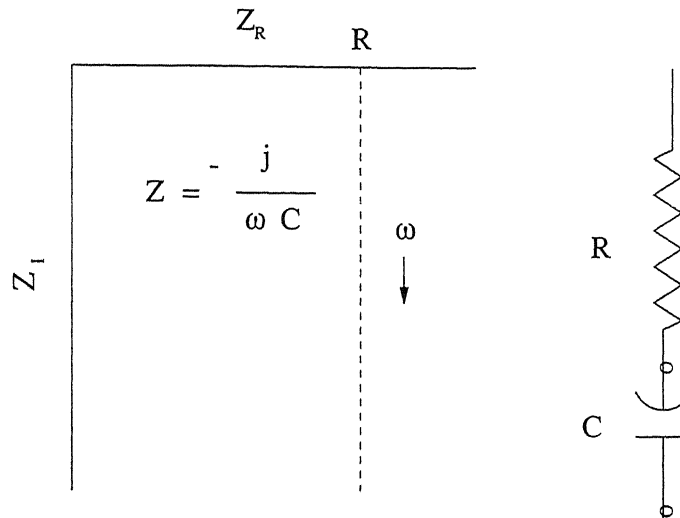


Fig. 2.1(c)

Fig. 2.1(c): Impedance plot for a resistor and a capacitor in series

#### 2.2.4 Parallel Combination of R and C:

If the system can be modeled as a resistor and a capacitor in parallel, then we have

$$Z^* = \frac{R \cdot (\frac{1}{j\omega C})}{R + (\frac{1}{j\omega C})} \quad (2.20)$$

$$(2.21)$$

$$= \frac{R}{1 + \omega^2 C^2 R^2} + j[-\frac{\omega C R^2}{1 + \omega^2 C^2 R^2}] \quad (2.22)$$

Thus the real and imaginary parts of the complex impedance are now

$$Z'' = \frac{R}{1 + \omega^2 C^2 R^2} \quad (2.23)$$

$$Z' = -\frac{\omega C R^2}{1 + \omega^2 C^2 R^2} \quad (2.24)$$

Eliminating  $\omega$  between these two equations, Eqs.2.21 and 2.22, we get

$$Z'^2 + Z''^2 = RZ' \quad (2.25)$$

$$(2.26)$$

$$\text{or} \quad (Z' - \frac{R}{2})^2 + Z''^2 = (\frac{R}{2})^2 \quad (2.27)$$

which is the equation of a circle of radius  $R$  with its centre at  $(Z' = R/2, Z'' = 0)$ . Essentially, the diameter of the circle is thus the dc resistance of the the sample.

The plots shown in Figs. 2.1(a-d) can be obtained only when non-blocking electrodes are used. When blocking electrodes, i.e., electrodes different from the constituents of the electrolyte, are used, the additional interface capacitance ( $C_{int}$ ) comes into picture due to polarization. In such a case, apart from semicircle, an inclined straight line especially at the lower frequencies, is also obtained for perfectly smooth surfaces (Fig. 2.2(a)).

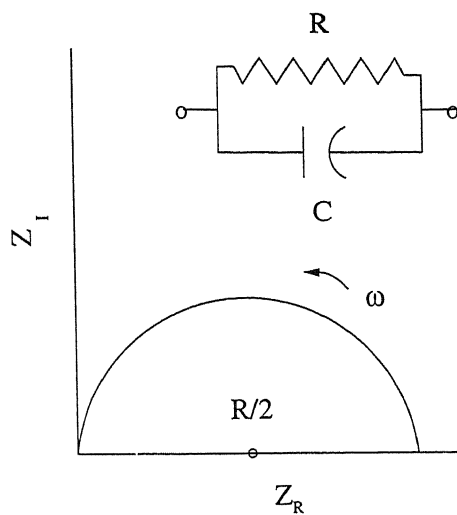


Fig. 2.1(d)

Fig. 2.1(d): Impedance plot for a resistor and a capacitor in parallel

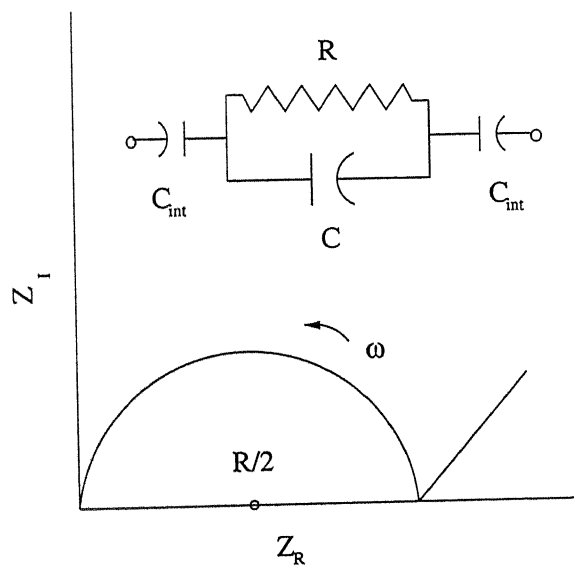


Fig. 2.2(a)

Fig. 2.2(a): Effect of interface capacitance  $C_{int}$  on impedance of electrolyte

In some cases, whenever multiple polarization is much effective, one gets a depressed semicircle, i.e., a part of the circle with centre lying at a point lower than the real axis. The diameter is taken as the measure of the dc resistance of the sample. Here CMP is the capacitance corresponding to multipole polarization (Fig. 2.2(b)).

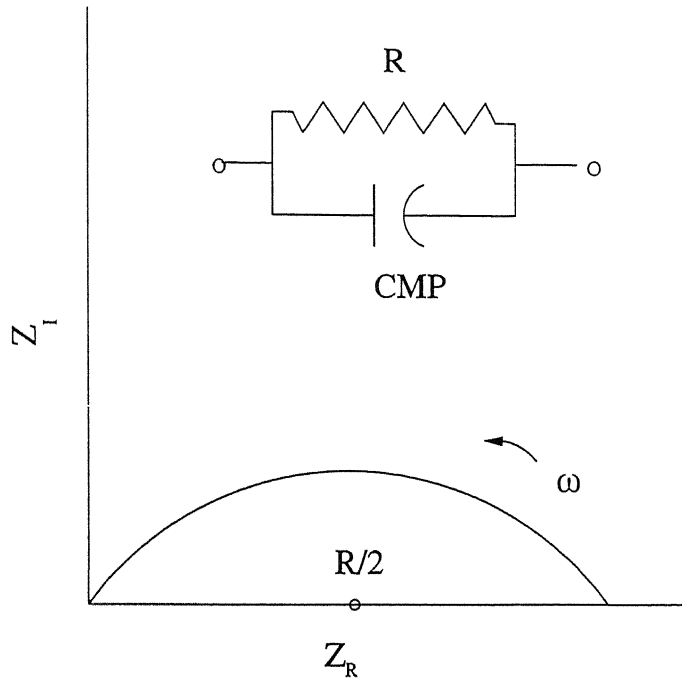


Fig. 2.2(b)

Fig. 2.2(b): Depression of semicircle due to multipole polarization

In poly-crystalline materials, ionic conduction may occur via the grain-boundaries besides the usual bulk conduction. Accordingly in some cases the impedance plot exhibits two semicircles as in Fig. 2.2(c). Thus the impedance analysis enables the separation of bulk and grain boundary conductivities.

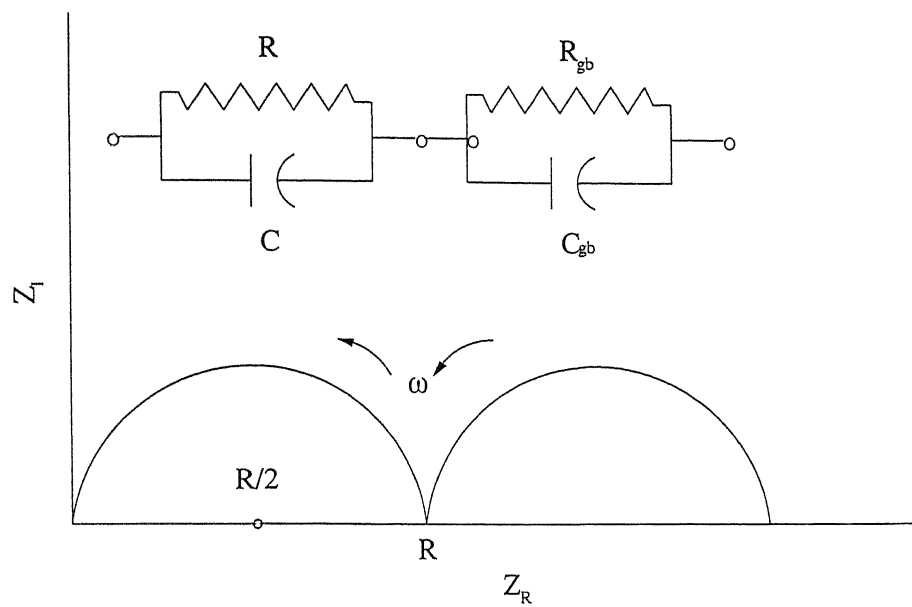


Fig. 2.2(c)

Fig. 2.2(c): Grain boundary effect

## 2.3 Experimental Set-up

The block diagram of the experimental set-up used for impedance measurement is shown in Fig. 2.3. The material under test, shaped as a cylindrical pellet, is placed in between the two stainless steel discs. Silver wires brazed to the steel discs serve the purpose of input leads to the impedance analyzer. The chromel-alumel thermocouple is used to measure the temperature of the sample. A special type of sample holder was fabricated to place the pellet along with the thermocouple inside the furnace. A temperature controller (Indotherm 401 D) was employed to control the furnace temperature. A Keithley (model Autoranging Microvolt DMM) digital multimeter was used to record the thermocouple voltage in millivolts.

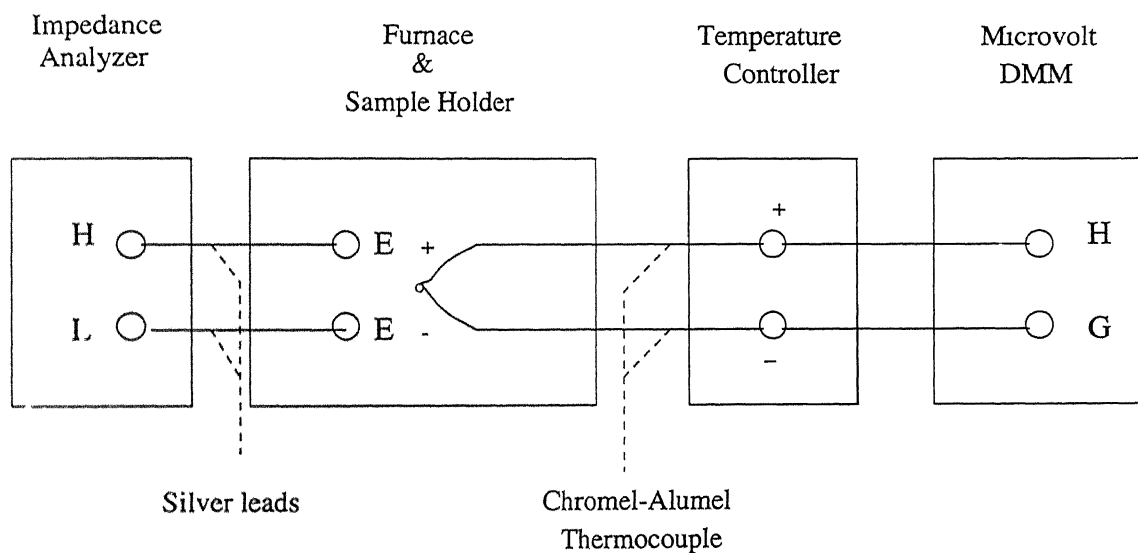


Fig. 2.3: Block diagram of the experimental set-up used in the ionic conductivity measurement

The various instruments and equipments that have been used in the set-up described above are being discussed below.

### 2.3.1 Sample Holder:

A sample holder as shown in Fig. 2.4 was fabricated for impedance measurement. It comprises of four properly sintered lava discs of about 2.5 cm diameter and 1.0 cm thickness. Each lava disc has five thru holes with of appropriate size, one at the centre and the remaining equally spaced along the periphery of the disc. Also there is (are) one (or two) small dip(s) of 0.1 cm depth and 1.2 cm diameter at the centre of the disc on one (or both) face(s). The sample pellet is placed between two stainless steel electrodes which in turn were spot welded to nichrome wires which would complete the circuit to the impedance analyzer for measurements. The nichrome wires were taken out through the holes of the lava discs. The sample and the electrodes were held between two discs with help of a spring. The other two discs formed the hot ends of the holder (put in the furnace). The other end was separated from the hot end at the ambient temperature, formed again by two discs with a stainless steel spring between them by a 20 cm long quartz tube (dia.=1.1cm). The discs were joined and mechanically supported by two ends threaded rigid stainless steel rods extended through the holes of the discs. Both ends of the stainless steel rod were bolted tightly to the respective discs at both ends and the spring transmitted the pressure uniformly on to the discs which ensured sufficient contact between the electrodes and the sample.

### 2.3.2 Furnace and Temperature Controller:

An electrical resistance heating furnace comprising of a mullite tube with internal diameter of  $\sim 1.5$  inch has been used. A high temperature cement was applied over the kanthal winding to keep it in its place. The mullite tube with cemented kanthal wiring was enveloped with a cylindrical stainless steel container and the annular space between the two shells was filled with MgO powder in order to minimize the heat loss.

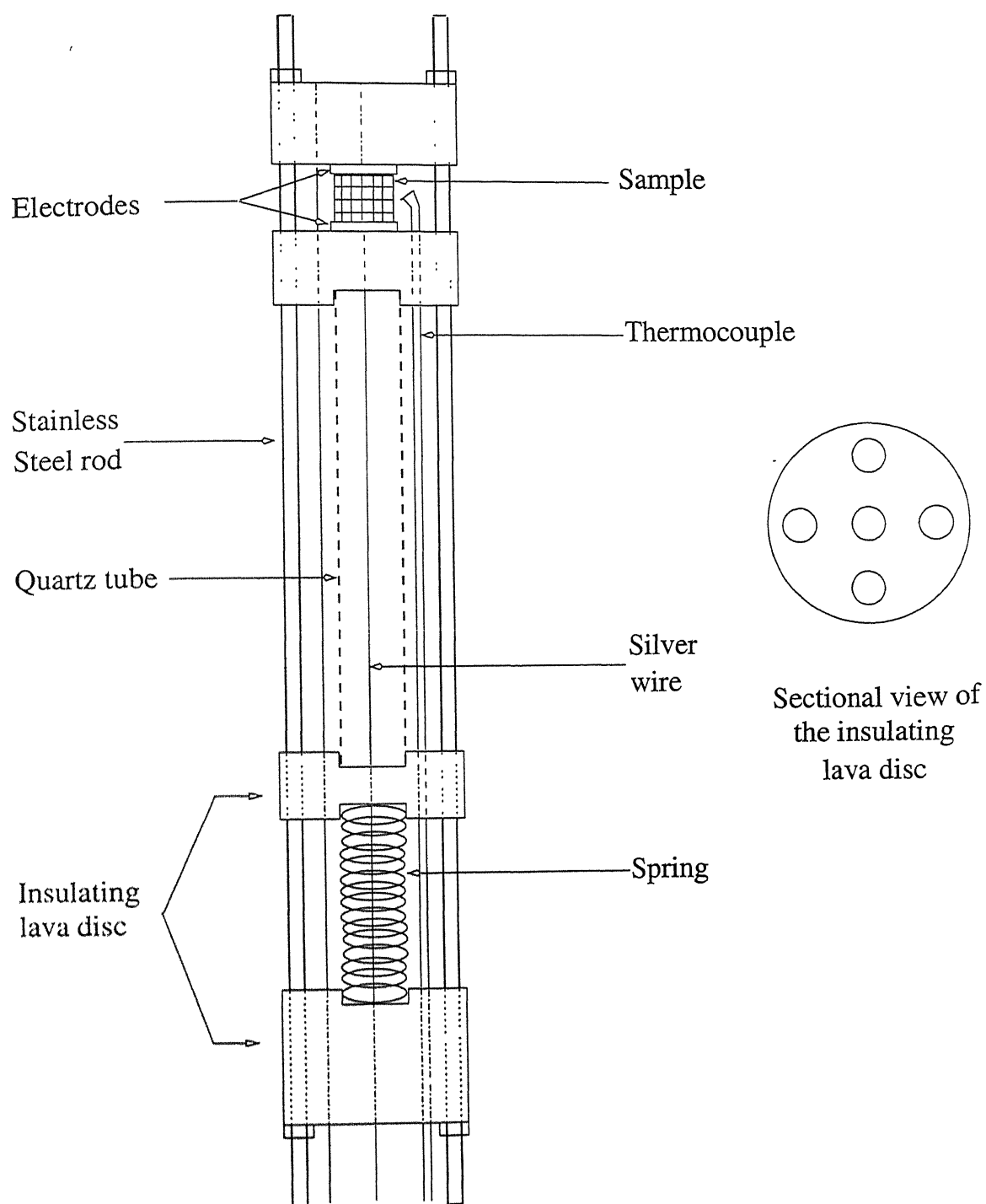


Fig. 2.4: Sample holder for impedance measurement



A chromel-alumel thermocouple with its junction kept very close to the sample, has been used to measure the temperature of the sample, as described earlier.

A PID type temperature controller (Indotherm 401D) has been used to control the temperature of the furnace.

### 2.3.3 Impedance Analyzer:

Impedance analyzer is a small-signal ac measurement device with a wide range of frequency to investigate the electro-chemical properties of the solid electrolytes. An HP 4192A impedance analyzer has been used. The instrument has an auto balancing bridge with a test signal from 5mV to 1.1 V. One can sweep the frequency from 5 Hz to 13 MHz. The two displays 'A' and 'B' display the associated pairs such as:

**Table 2.1: The displays 'A' and 'B' of the Impedance Analyzer**

A	B
Complex impedance (Z)	Phase angle $\theta$
Admittance (Y)	(deg or rad)
Resistance (R)	Reactance (X)
Conductance (G)	
Inductance (L)	Q-factor
Capacitance (C)	D-value

. One can select any pair of interest in either series or parallel mode.

## 2.4 Materials Processing

The physical and chemical properties of the three starting materials, viz, the glass former ( $\text{B}_2\text{O}_3$ ), the glass modifier ( $\text{Li}_2\text{O}$ ) and the salt ( $\text{Li}_2\text{SO}_4$ ), are summarized in the following Table.

**Table 2.2:** The physical and chemical properties of the starting materials

Informations	$\text{B}_2\text{O}_3$	$\text{Li}_2\text{O}$	$\text{Li}_2\text{SO}_4$
Obtained from	Loba Chemie	Aldrich	Aldrich
Purity	-	99%	99%
Physical Properties			
Molecular weight (gm.)	69.62	29.88	109.94
Density (gm/cc)	2.46	2.013	2.221
Melting point ( $^{\circ}\text{C}$ )	450	1200	845
Boiling point ( $^{\circ}\text{C}$ )	1860	>1700	-
Chemical Properties			
Important notes/ Caution	chemically inactive	corrossive, hygroscopic, absorbs $\text{CO}_2$	harmful, hygroscopic, possible tetragon

Table 2.3 below gives the composition of five different samples which are investigated in this work.

**Table 2.3: The compositions of the samples investigated**

Sample	Molar Ratio $\text{Li}_2\text{SO}_4 : \text{Li}_2\text{O} : \text{B}_2\text{O}_3$	Weight (gm.)		
		$\text{Li}_2\text{SO}_4$	$\text{Li}_2\text{O}$	$\text{B}_2\text{O}_3$
dopant salt	100:0:0	4.0	-	-
host system	0:75:25	-	2.2514	1.7486
S50	50:37.5:12.5	2.9365	0.5986	0.4649
S40	40:45:15	2.5920	0.7925	0.6155
S30	30:52.5:17.5	2.1681	1.0312	0.8007
S20	20:60:20	1.6301	1.3339	1.0360
S10	10:67.5:22.5	0.9391	1.7228	1.3381

#### 2.4.1 Synthesis of Glasses:

The starting materials in appropriate ratios were mixed thoroughly in an agate mortar and pestle. The grinding resulted in a very fine-powdered mixture. The ground powder was then taken in an alumina crucible which in turn was placed inside the furnace. The temperature is then increased slowly till the mixture melts. The melting points of the mixtures were found to be in the range 750 - 850 °C. The temperature of the furnace was usually maintained at about 40K above the melting points of the respective materials for one hour duration in order to homogenize the melt.

Two copper blocks precooled at  $\sim 77\text{K}$  (using liquid nitrogen) were used for quenching. The alumina crucible was quickly taken out of the furnace and the melt

poured on to one of the precooled copper plates and pressed by the other plate. In this quenching process, the expected cooling rate is  $\sim 10^{+3}$  °C/S. The formation of glass depends upon the cooling rate, and thus bringing the melt out and subsequently pouring it on to the copper block were completed in the least possible time. The glasses formed on the copper plate were very thin, transparent and colorless. Lesser the thickness, better is the quality of the glass.

The formation of the glass and its quality were checked by XRD measurements. For this purpose, a small amount of the quenched material was powdered and used to obtain XRD data. It was observed that if the quenching process was not carried out swiftly and properly, the resulting material was more like a mixture of glass and some crystalline substance. In all seven samples of various compositions, three of which are glasses, three partially glass and one ( $\text{Li}_2\text{SO}_4$ ) crystalline salt, have been used for electrical characterization

#### **2.4.2 Pelletization and Electrodes:**

The quenched material was ground a slightly and very gently, because high grinding pressure may cause crystallization of the glassy phase. This of course was easily achieved since the glassy product was very soft and thin. After grinding, it was then transferred into a stainless steel die. The die was placed under a hand-operated hydraulic press. A pressure of 4 tons was applied on the die for a couple of minutes. Then having released the pressure the pellets were taken out. The diameter of the pellets were fixed by that of the die, ( $\sim 11$  mm). The thicknesses of the pellets ranged from 2.3 - 3.8 mm.

For electrical measurements, graphite was used as electrode. Two different techniques were employed. In one case, the graphite paint was used. Both the flat surfaces of the pellets were painted and dried up consecutively. In the second case,

the graphite powder was used at the time of making pellet itself. In this case, equal and known amounts of graphite powder were taken in the die both before and after the quenched material, so that the pellet was released from the die along with the electrodes. A known amount of graphite powder was used to make a graphite pellet in order to determine the thickness of the sample without graphite.

The surface resistances of the electrodes were usually measured to check whether they were sufficiently conducting. For graphite paint it was  $10\text{-}20\Omega$  while for graphite powder it was found to be  $5\text{-}10\Omega$ .

## 2.5 Impedance Measurement

HP 4192A impedance analyzer, was used to measure the impedance  $Z$  and the phase angle  $\theta$ . The frequency was swept from 5Hz to 13MHz for each temperature, and the temperature was varied from 25°C (room temp) to higher temperatures above the glass transition temperature  $T_g$ . While collecting impedance data, attention was paid to detect the change of smooth behavior of impedance value  $Z$ . It has already been discussed that the ionic conductivity of the glasses follow the Arrhenius equation in the glassy state while it becomes non-Arrhenius type when heated above the transition temperature. Thus the  $\log \sigma$  versus  $10^3/T$  plot is linear in the glassy state and it becomes non-linear when the temperatures higher than  $T_g$ . Therefore the transition temperature was determined while collecting data itself and this was taken as the upper limit of the temperature.

For dielectric measurement the displays can be set to 'C' and 'D' to obtain  $\epsilon'$  and  $\epsilon''$  and the dielectric loss  $\tan \delta$ . But as mentioned earlier the dielectric related quantities are possible to calculate, only  $Z$  and  $\theta$  were noted down. But for some frequencies all the quantities  $Z$ ,  $\theta$ , C and D values were collected and verified by calculating one pair from the other.

For example, capacitance C and dielectric loss D are related to complex impedance  $Z$  and phase angle  $\theta$  as mentioned below:

$$C = C_o \epsilon' \quad (2.28)$$

$$= \frac{\sin \theta}{\omega Z} \quad (2.29)$$

$$D = \frac{\epsilon''}{\epsilon'} \quad (2.30)$$

$$= \frac{Z'}{Z''} \quad (2.31)$$

$$= \cot \theta \quad (2.32)$$

After reaching  $T_g$ , the transition temperature, the temperature was kept con-

stant for some time and then it was cooled down slowly. The impedance data were collected in the cooling cycle also to get an idea of the conductivity of the crystalline state of the material.

All measurements were repeated for all the samples to check the reproducibility and reliability of the data

# Chapter 3

## Results & Discussion

As mentioned in the preceding Chapters, besides the glassy host  $\text{Li}_2\text{O} - 25 \text{ m/o } \text{B}_2\text{O}_3$ , five glass samples containing 10,20,30,40,50 mole % of the salt ( $\text{Li}_2\text{SO}_4$ ) in host (referred to as S10, S20, S30, S40, S50 here after) have been synthesized with a view to produce a  $\text{Li}^+$ -ion based superionic glass suitable for electrochemical applications. The XRD measurements have been carried out for their structural characterization, while impedance data as a function of frequency (5 Hz to 13 MHz) and temperature were taken to extract ac/dc conductivities, dielectric constant and loss, and associated activation energies/ relaxation parameters. These results are produced below.

### 3.1 X-ray Diffraction

The XRD patterns of the quenched materials as well as those of the corresponding mixtures (before heating) and starting materials have been taken, and the results are shown in Figs. 3.1(a-c). It is observed that the characteristic peaks of crystalline  $\text{Li}_2\text{SO}_4$  and  $\text{Li}_2\text{O}$  are still present in the quenched state but with much reduced intensity. It is therefore clear that the samples with higher concentration ( $x = 30$ ,



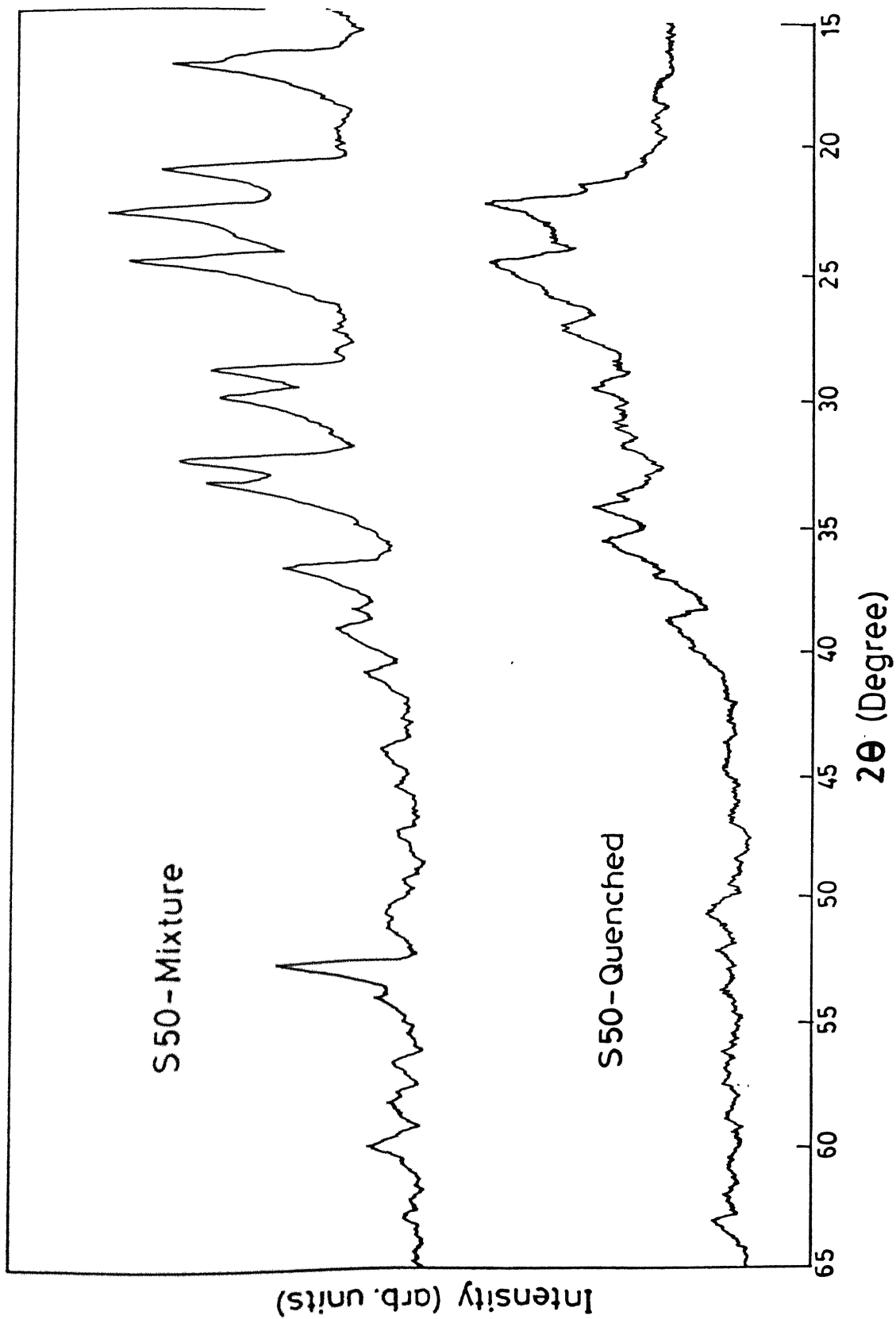


Fig. 3.1(a): XRD pattern for the crystalline mixture and quenched material for S50 sample

40, 50) are not entirely glassy. They retain the key structure of their crystalline constituents, mainly that of  $\text{Li}_2\text{SO}_4$ . Thus they are of partially crystalline nature. However it was possible to obtain completely glassy network for the S10, S20 besides the host system ( $x=0$ ). The XRD patterns for S20 composition and the host are shown in Fig. 3.1(c).

The host,  $\text{B}_2\text{O}_3 + 75 \text{ mol}\% \text{Li}_2\text{O}$ , is a pure glass. The samples containing  $\text{Li}_2\text{SO}_4$  upto 20 mol% form glassy network. This means that  $\text{SO}_4^{2-}$  ions introduced into the chosen LB system get diluted upto that molar ratio without any detectable reaction with the network<sup>[12,17]</sup>. If the molar percentage of  $\text{Li}_2\text{SO}_4$  is increased, however, it does not get dissociated in the glass matrix, as the  $\text{Li}_2\text{SO}_4$  peaks and in some cases one or two  $\text{Li}_2\text{O}$  peaks are observed in Fig. 3.1(a),(b).

Although due to the presence of  $\text{Li}_2\text{SO}_4$ , the glass network does not get affected fundamentally, <sup>[17]</sup> i.e., the orientation of the boroxol units etc. retain their glassy configuration, but the network gets stretched and thus causes more NBOs<sup>[21]</sup>. So there one can expect a better “dispersion” of BO-network. But 30 mol% or more  $\text{Li}_2\text{SO}_4$  results in insolubility of the same into the LB solvent, the composition with 20 mol% dopant salt can be considered as the optimised ratio for ionic conductivity and other related phenomena.

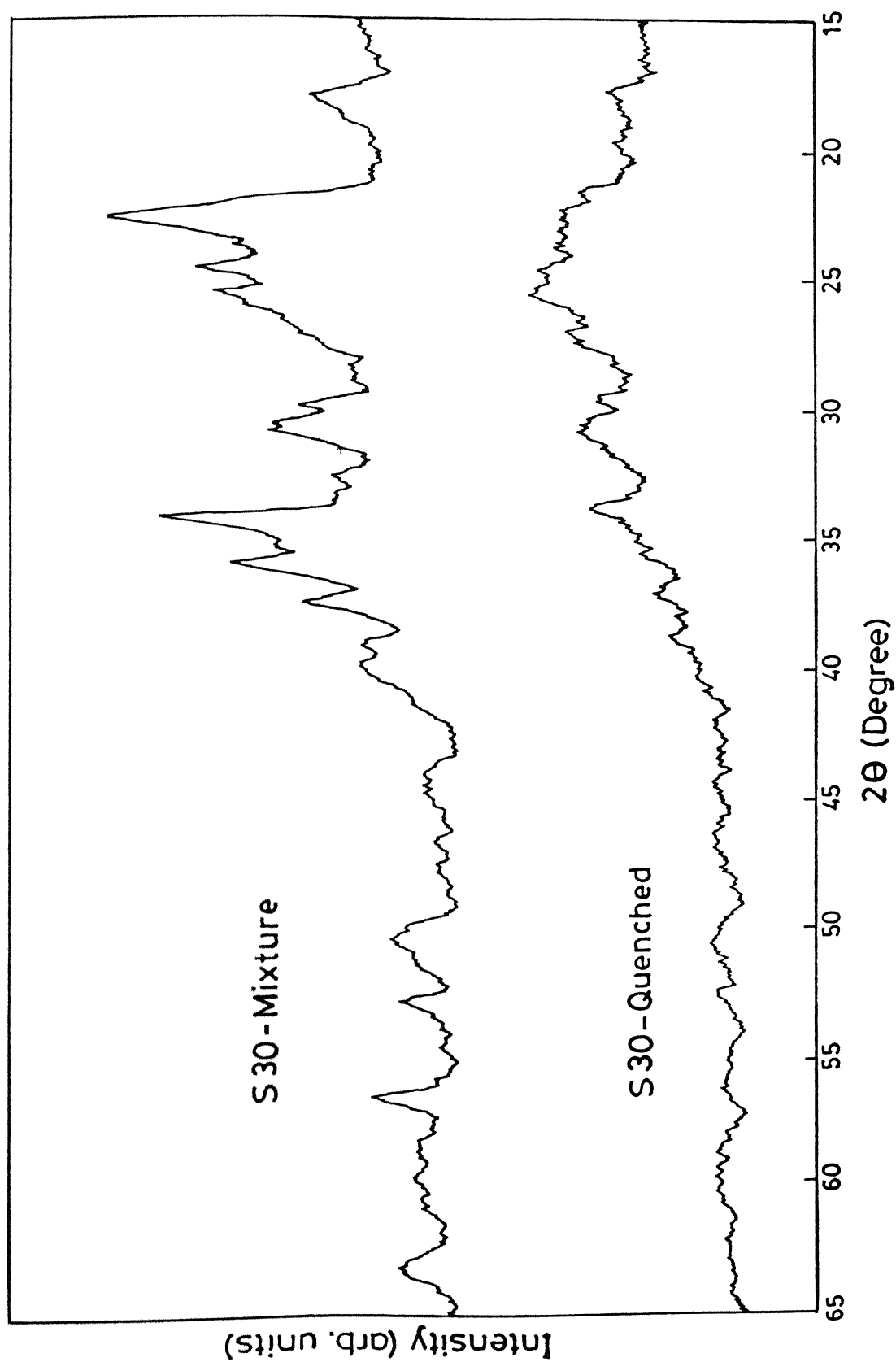


Fig. 3.1(b): XRD pattern for the crystalline mixture and quenched material for S30 sample

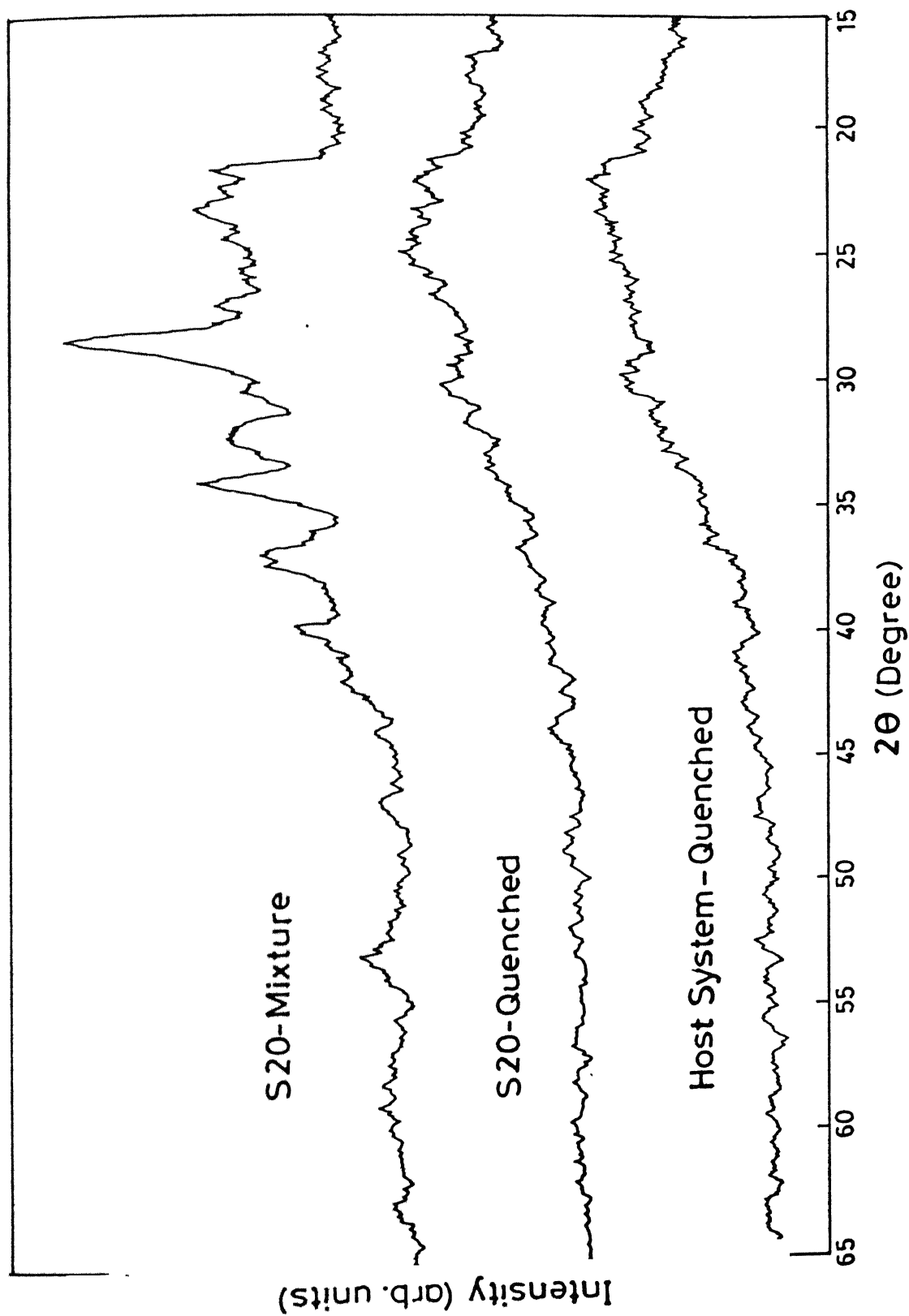


Fig. 3.1(c): XRD pattern for the crystalline mixture and quenched material for S20 sample and quenched host system

## 3.2 Impedance Analysis

The electrode/solid electrolyte assembly together with the lead wires represent a complex impedance ( $Z^*$ ). As discussed in the previous Chapter (2.2.4), the variation of the real and imaginary parts of the complex impedance as function of frequency is employed to obtain the dc resistance of the sample. The impedance plots for pure  $\text{Li}_2\text{SO}_4$  and sample S20 are shown in Figs. 3.2 (a)-(d) and Fig. 3.3 respectively.

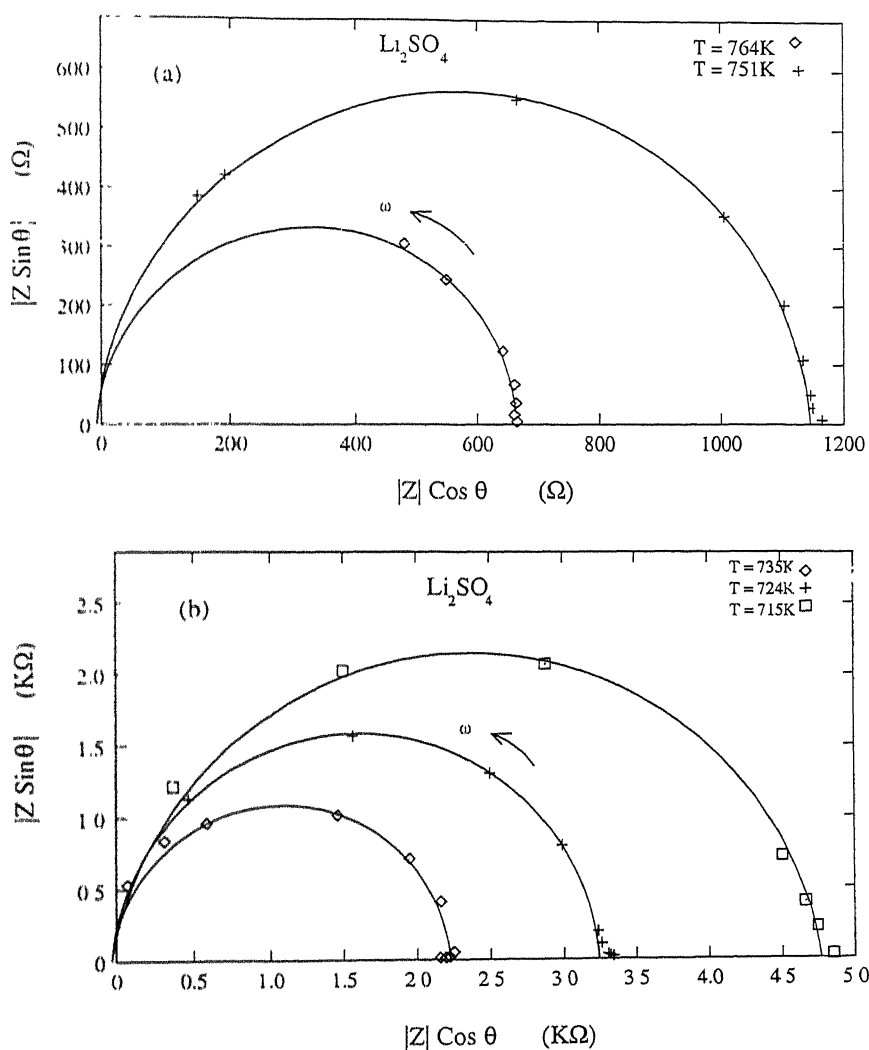


Fig. 3.2: Impedance plots for pure  $\text{Li}_2\text{SO}_4$  at (a) 751 and 764 K and (b) 715, 724, 735 K

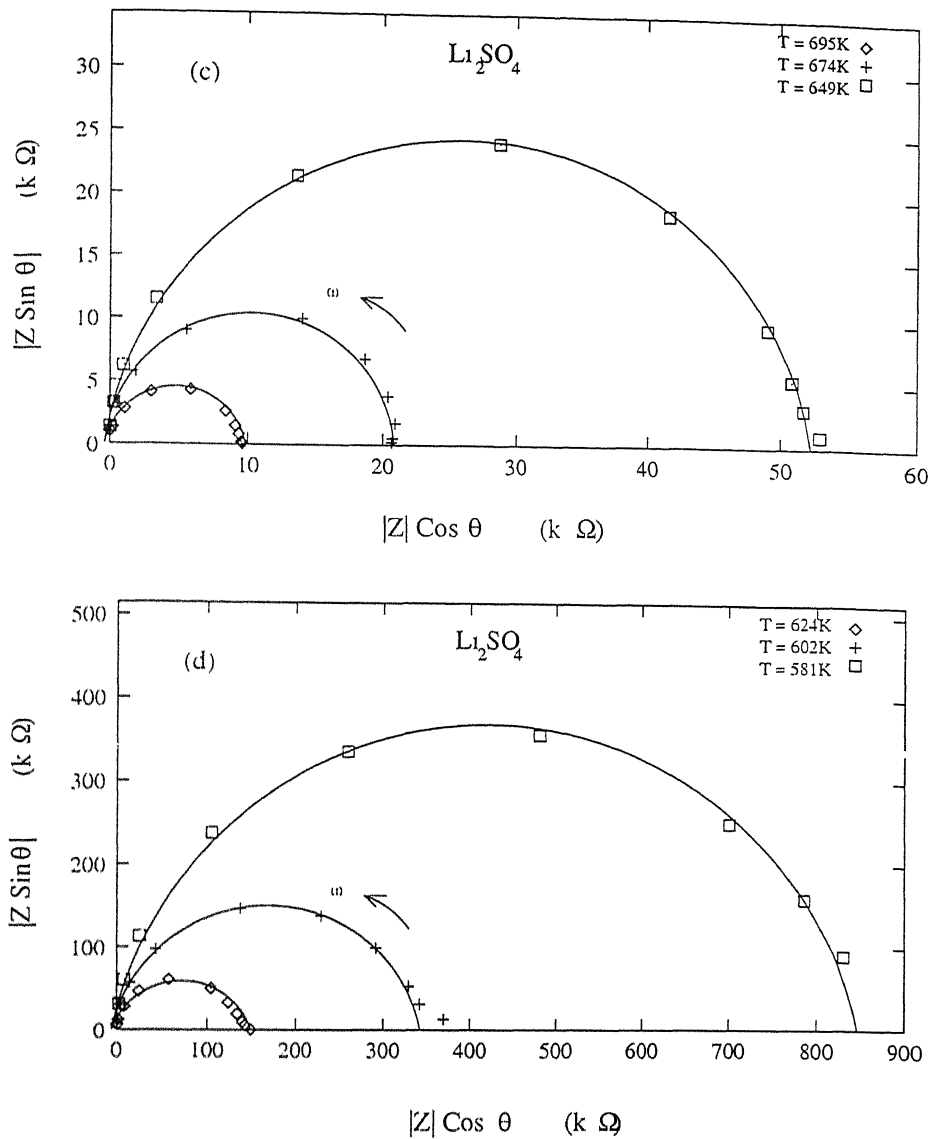


Fig. 3.2: Impedance plots for pure  $\text{Li}_2\text{SO}_4$  at (c) 649, 674 and 695 K and (d) 581, 602 and 624 K

As observed in Figs. 3.2(a-d) the are, within experimental error, good semi-circles, which essentially implies that the sample/electrode assembly behaves like a true parallel combination of a resistor and a capacitor. In all such cases, the diameter of the semicircle yields the dc resistance and hence the dc conductivity

However, in some cases only a part of the circle is obtained, which can be considered as depressed semicircles whose centre lies below the real axis of the impedance plots. This is the situation where the sample/electrode assembly does not behave like a parallel combination of a resistor and a capacitor. This fact is more dominant in the glassy ionic materials used in the present investigation. Fig 3.3 shows the impedance plots for the glassy sample S20. It was observed that higher the temperature, more is the depression. This indicates that as temperature increases and the sample becomes more conducting, the interfacial polarization becomes more dominant.

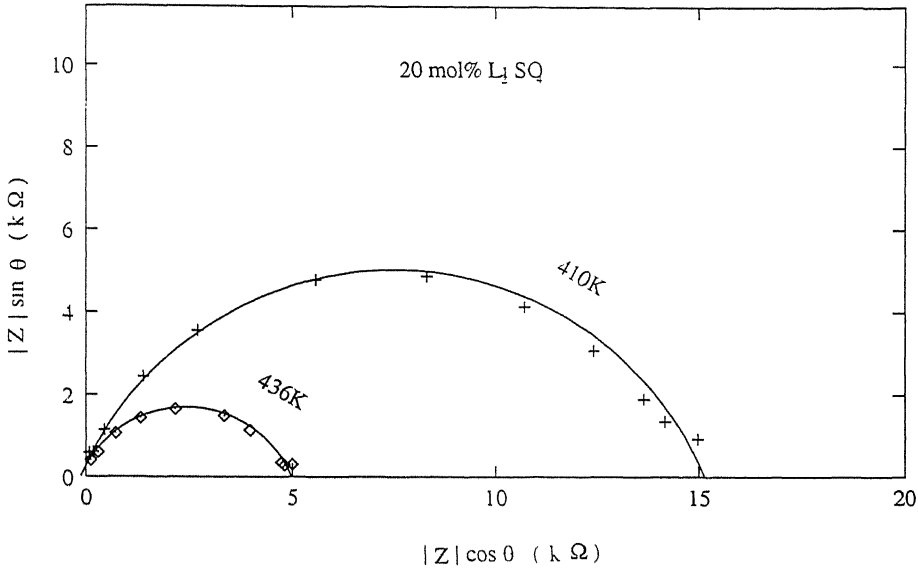


Fig. 3.3: Impedance plot for 20 mol%  $\text{Li}_2\text{SO}_4$  glass composition at 410 and 436 K

At low temperatures, the phase angle  $\theta$  does not change appreciably and thus a straight line is obtained. Here the phase angle lies in the range  $70-90^\circ$ . Also at very high temperatures, near  $T_c$ , the available frequency range is too limited to produce the full semicircles.

### 3.2.1 DC Conductivity:

In order to determine the dc conductivity, the diameter of the semicircles have been taken as a measure of dc resistance of the sample following the parallel combination model described in Chapter 2. The dc conductivity is then calculated using the following simple relation

$$\sigma = \frac{l}{R.A} \quad (3.1)$$

where  $R$  denotes the resistance of the sample (or the diameter of the semicircles in the impedance plots, Figs. 3.2 and 3.3),  $l$  is the thickness of the pellet and  $A$  represents the cross-sectional area of the flat surfaces of the pellet.

The contributions to resistivity due to other components like electrodes, lead wires etc. are negligible compared to that of the solid electrolyte.

Wherever semicircles are not obtainable within the available frequency range (5Hz - 13Hz) of the impedance analyzer, in general, the ac conductivity at 1kHz is used instead of the dc one. The ac conductivity is calculated using the relation

$$\sigma_{ac} = \frac{l}{Z(\omega).A} \quad (3.2)$$

where  $Z(\omega)$  is the impedance at analyzer frequency  $\omega$ . Generally, the ac conductivity at a lower frequency of 5kHz is reported in this work. However, it may be pointed out that the ac conductivity at lower frequencies is almost independent of frequencies (see Fig. 3.4) except at lower temperatures.



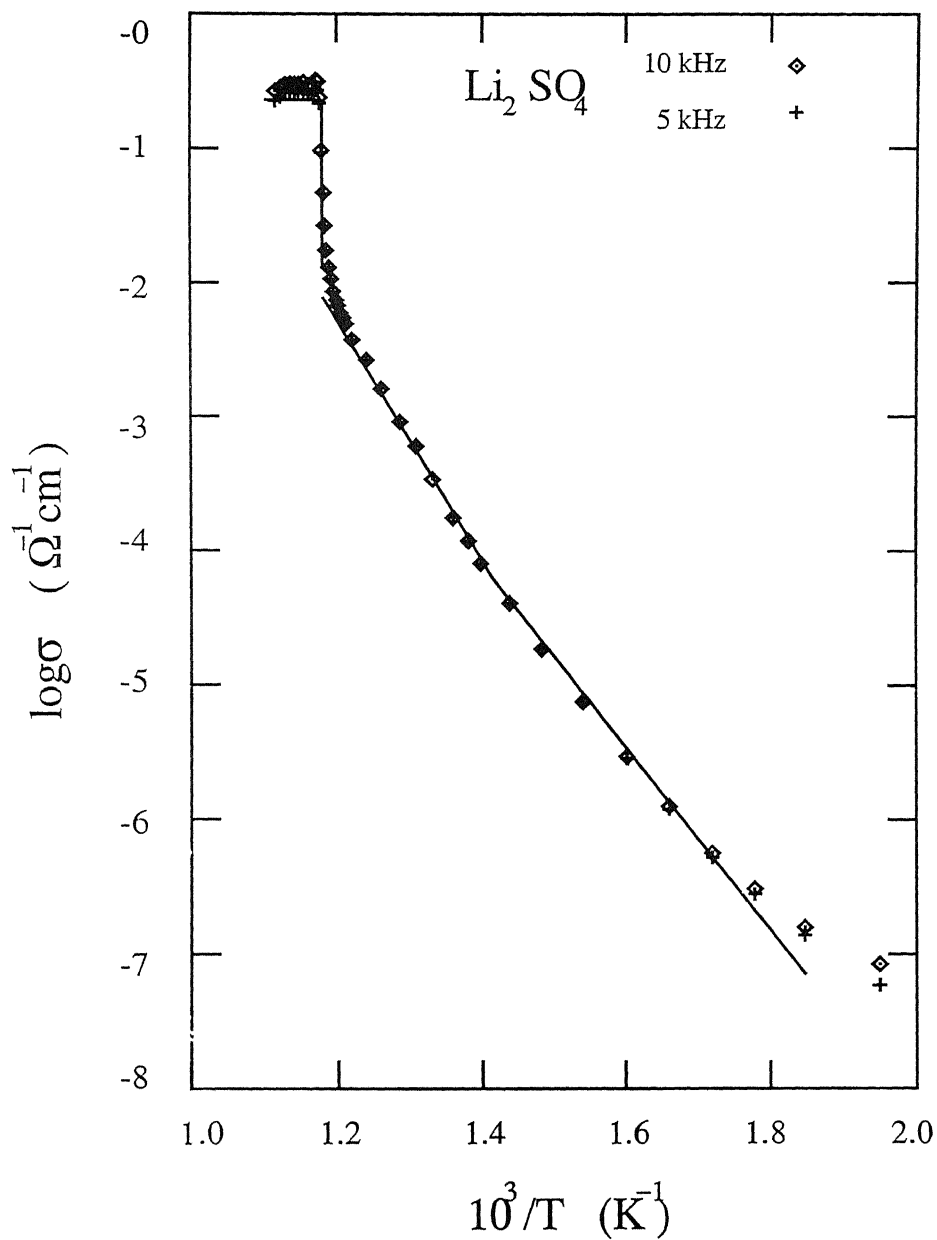


Fig. 3.4: Logarithm of ac conductivity vs. inverse temperature plot for pure  $\text{Li}_2\text{SO}_4$  at two different frequencies 5 and 10 kHz.

### 3.3 Electrical Conductivity Vs Temperature

The aim of the present investigation was to search for a glassy superionic material for possible use as a good solid electrolyte in cells and batteries. In this Section, the variation of ionic conductivity with temperature has been discussed.

#### 3.3.1 Pure $\text{Li}_2\text{SO}_4$ :

In the chosen glassy system,  $\text{Li}_2\text{SO}_4\text{-Li}_2\text{O-B}_2\text{O}_3$ , the dopant salt  $\text{Li}_2\text{SO}_4$  is supposed to contribute the mobile  $\text{Li}^+$  ions, and thus to an extent control the conductivity of the system. It is therefore desirable to study the electrical conductivity of the dopant salt itself. Fig. 3.5 shows these results.

It is observed that the logarithm of conductivity increases most linearly, as expected. Since the  $\text{Li}_2\text{SO}_4$  used in this work is a nominally pure polycrystalline sample owing to impurities already present in the sample, the  $\log\sigma$  vs  $10^3/T$  plot exhibits the well known features such as (low temperature) extrinsic region and a (high temperature) intrinsic region. The so called knee temperature separating the two regions at  $T_N = 715$  K (442 °C). Further, the migration energy from the slope at lower temperatures is found to be 1.43 eV. The high temperature (intrinsic region) activation energy of  $\sim 2.00$  eV would thus yield 1.14 eV for the formation energy of defects in  $\text{Li}_2\text{SO}_4$ . The values of formation and migration energies are generally in good agreement with literature.<sup>[23]</sup>

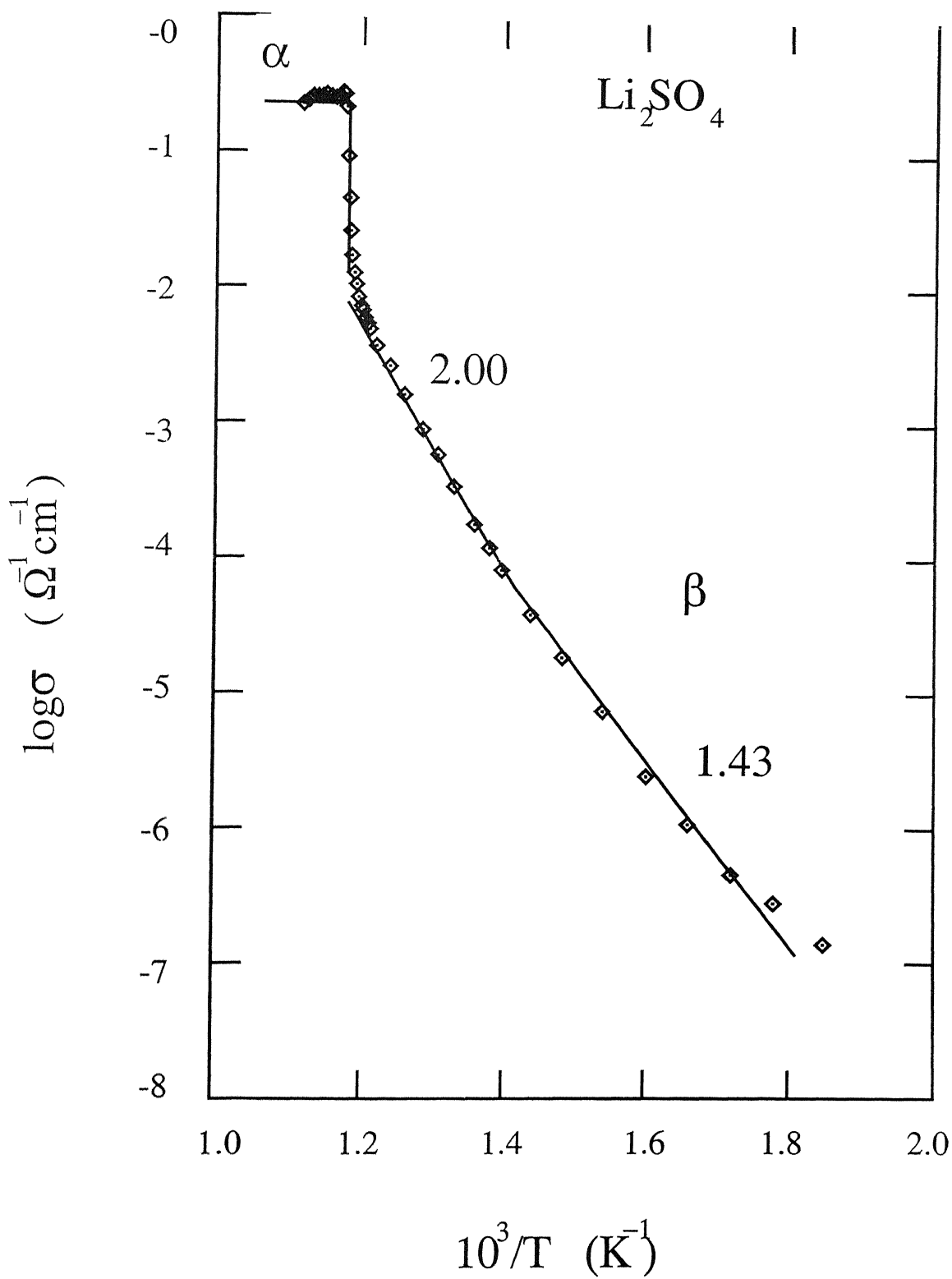


Fig. 3.5: Logarithm of dc conductivity vs. inverse temperature plot for pure  $\text{Li}_2\text{SO}_4$

The sharp change in the conductivity at  $\sim 843$  K is due to  $\beta$ - $\alpha$  phase transition in  $\text{Li}_2\text{SO}_4$ . The conductivity in the (superionic) phase is of the order of  $0.28 \Omega^{-1}\text{cm}^{-1}$ . Above this transition temperature, the conductivity remains practically constant, like those of molten salts/aqueous solutions.

Table 3.1 summarizes the relevant transport parameters corresponding to the different phases of  $\text{Li}_2\text{SO}_4$ .

**Table 3.1:** Characteristic features of pure  $\text{Li}_2\text{SO}_4$ :

Temperature (K)		Conductivity ( $\Omega^{-1} \text{ cm}^{-1}$ )	Energy (eV)		
Knee $T_N$	Transition $T_c$		migration $g_m$	activation $E_a$	formation $g_f$
715 (442°C)	843 (572°C)	0.28 ( $T > T_c$ )	1.43	2.00	1.14

### 3.3.2 The Host System:

As discussed in Chapter 1, the present system can be looked as a solution where LB system is the solvent. Our interest includes the understanding of the effect of addition of the solute  $\text{Li}_2\text{SO}_4$  in the solvent, the host system. Therefore it is also very essential to know the characteristics of the LB system separately. Those are shown in Fig. 3.6. It may be observed that the conductivity of the host system is relatively high, as expected, due to the presence of  $\text{Li}_2\text{O}$  in large proportion.

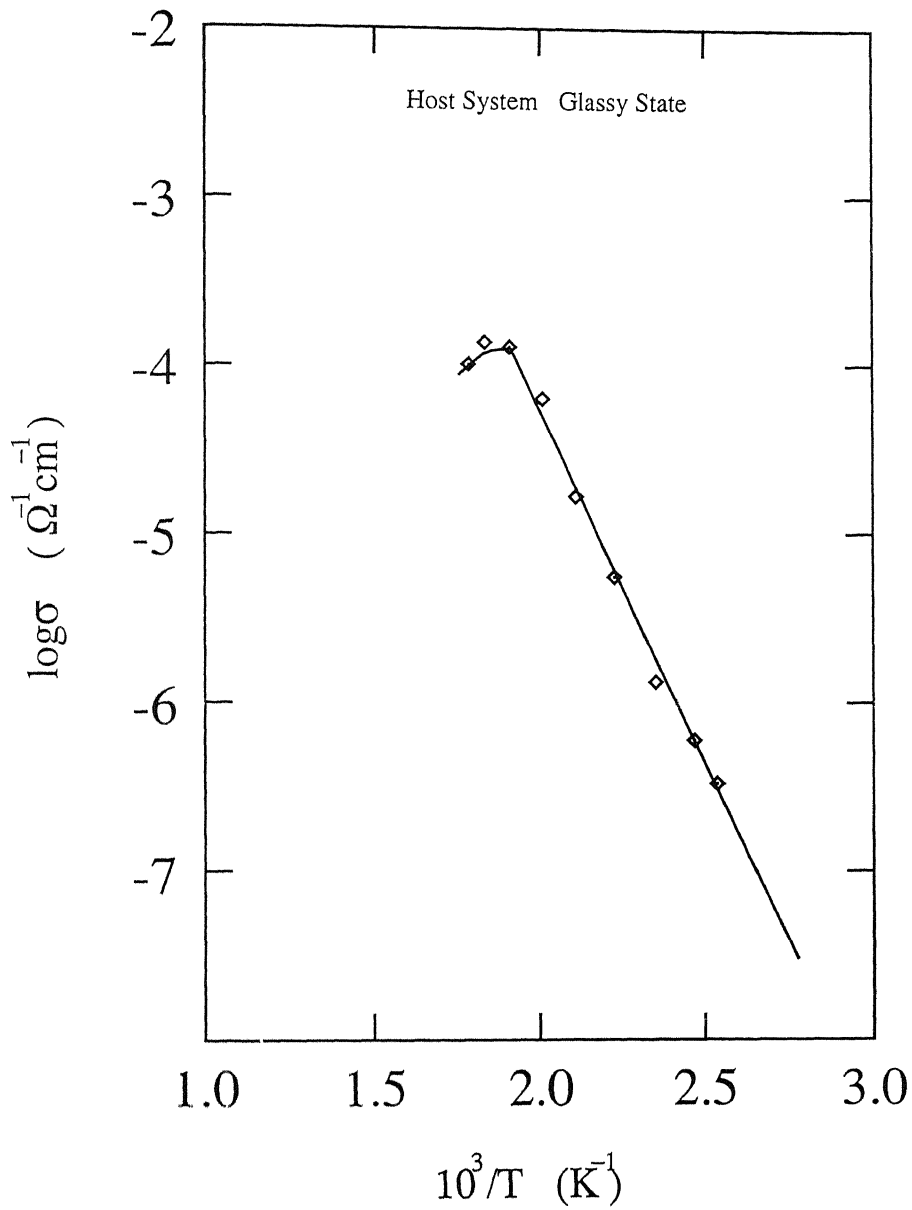


Fig. 3.6: Logarithm of dc conductivity vs. inverse temperature plot for host system,  $\text{Li}_2\text{O} + 25 \text{ m/o B}_2\text{O}_3$

$\text{Li}_2\text{O}$  has contributed  $\text{Li}^+$  ions to the glass matrix and those ions are responsible for such a high ionic conductivity. This can be mentioned that keeping this in view, the host was chosen with such a high fraction of  $\text{Li}_2\text{O}$ .

### 3.3.3 Glasses:

As already mentioned, the samples with 30,40 and 50 mol%  $\text{Li}_2\text{SO}_4$  are not completely glass but a mixture of glass and crystalline materials. However, the samples of composition 20 and 10 mol%  $\text{Li}_2\text{SO}_4$  form perfect glass. The electrical conductivity as a function of inverse temperature for these pure glassy systems, have been shown in Figs. 3.7 and 3.8. The samples were first heated up and then cooled down

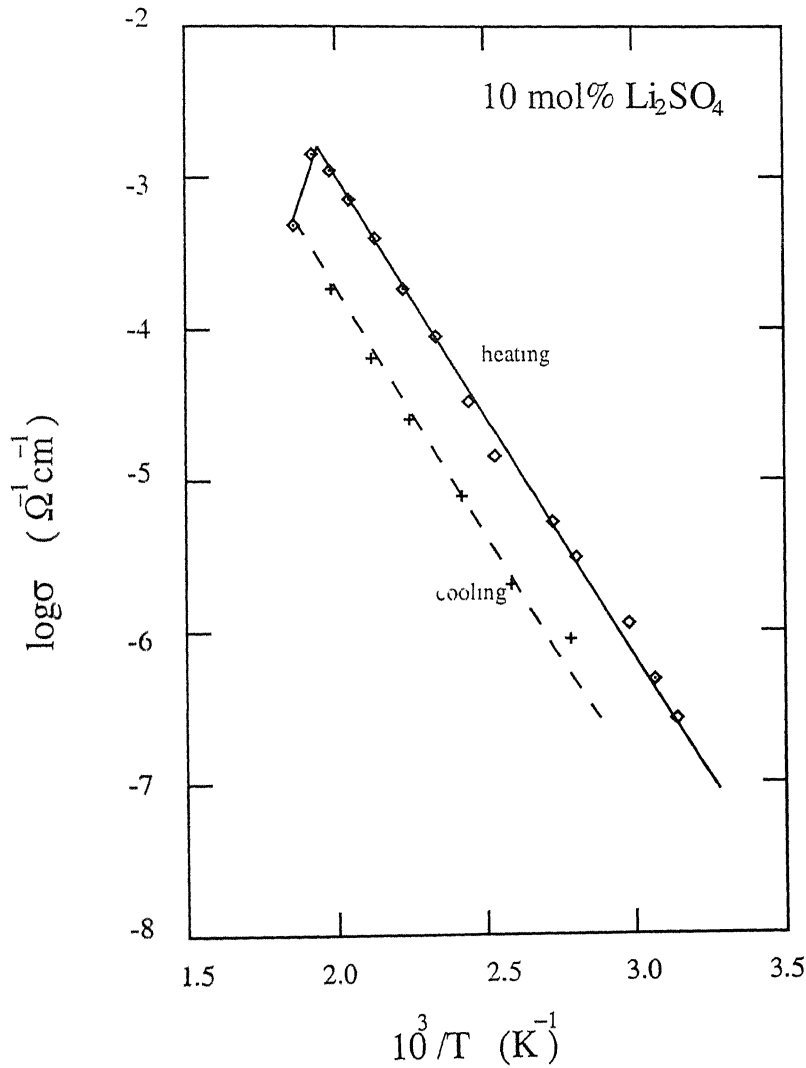


Fig. 3.7: Logarithm of dc conductivity vs. inverse temperature plot for 10 mol%  $\text{Li}_2\text{SO}_4$  glass (sample S10)

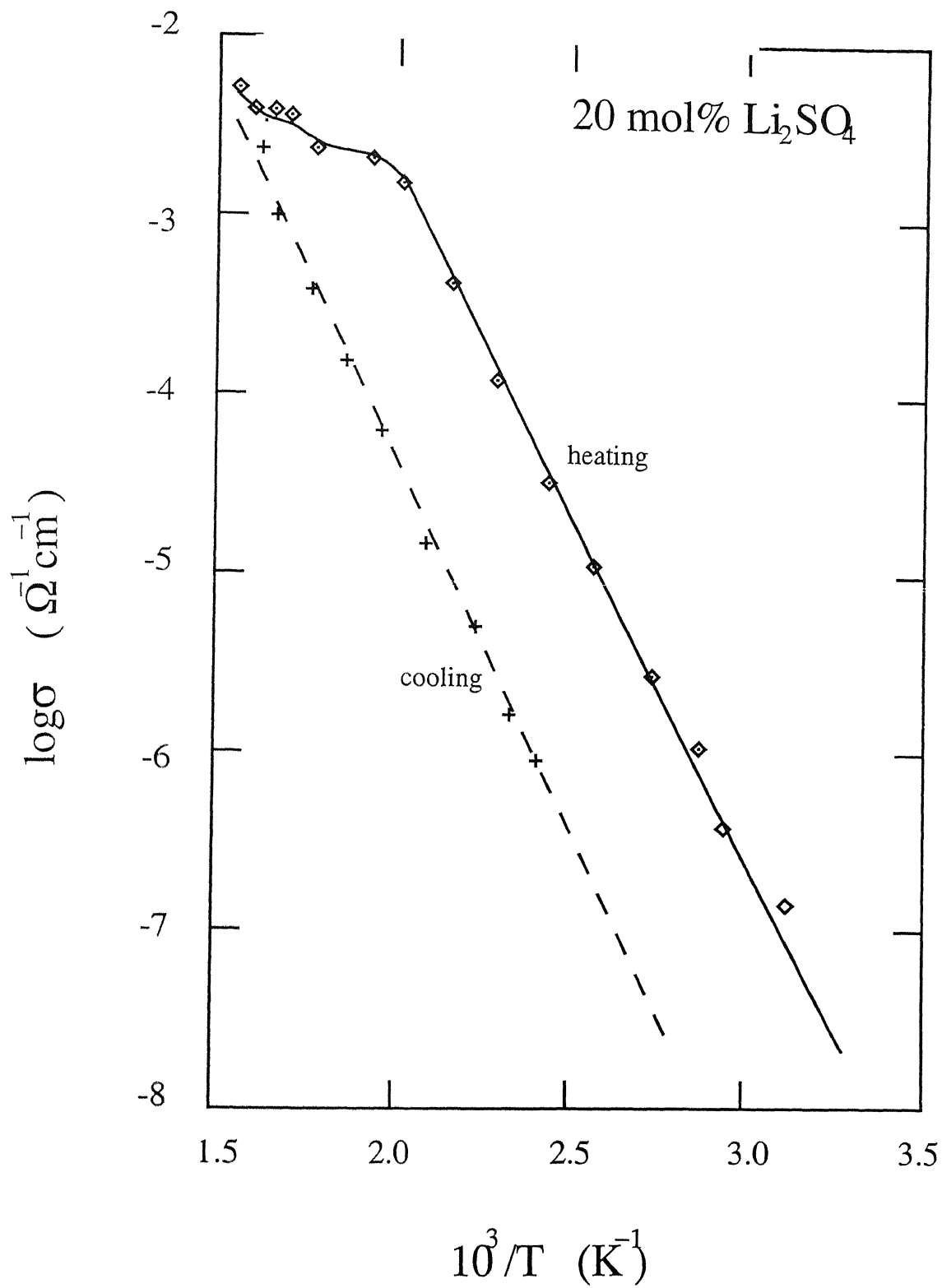


Fig. 3.8: Logarithm of dc conductivity vs. inverse temperature plot for 20 mol%  $\text{Li}_2\text{SO}_4$  glass (sample S20)

The heating cycle data essentially correspond to the glassy state of the sample.

It is observed that the conductivity vs. inverse temperature dependence follows Arrhenius law. There is no change in the slope in the glassy state. Since the glass is a disordered state with a large number of built-in defects, the activation energy obtained from the single slope of linear  $\log \sigma$  vs.  $10^3/T$  plot may be taken as migration energy of the  $\text{Li}^+$  ions. In this manner, the migration energies 0.65 and 0.60 eV are found for 10 and 20 mol%  $\text{Li}_2\text{SO}_4$  samples. However as temperature increases, the nature of the linear curve changes above a certain temperature. There is appreciable departure from the linear behavior which may be attributed to glass  $\rightarrow$  crystalline transition. The temperature at which the sample starts showing non-linear behavior is a measure of transition temperature<sup>[24]</sup> (denoted by  $T_g$ ). After reaching  $T_g$  the conductivity data for cooling cycle were also measured to know its nature in crystalline state. As clearly seen here, the glassy state conductivity is much higher ( $\sim 10^2$ ) than that in the crystalline one.

To check the reproducibility of the glassy state, the experiment was repeated before crossing the transition temperature  $T_g$ . This has been shown in Fig. 3.9 for S20. The cooling cycle measurements follow the same path as that for the heating cycle for the material remains glassy.



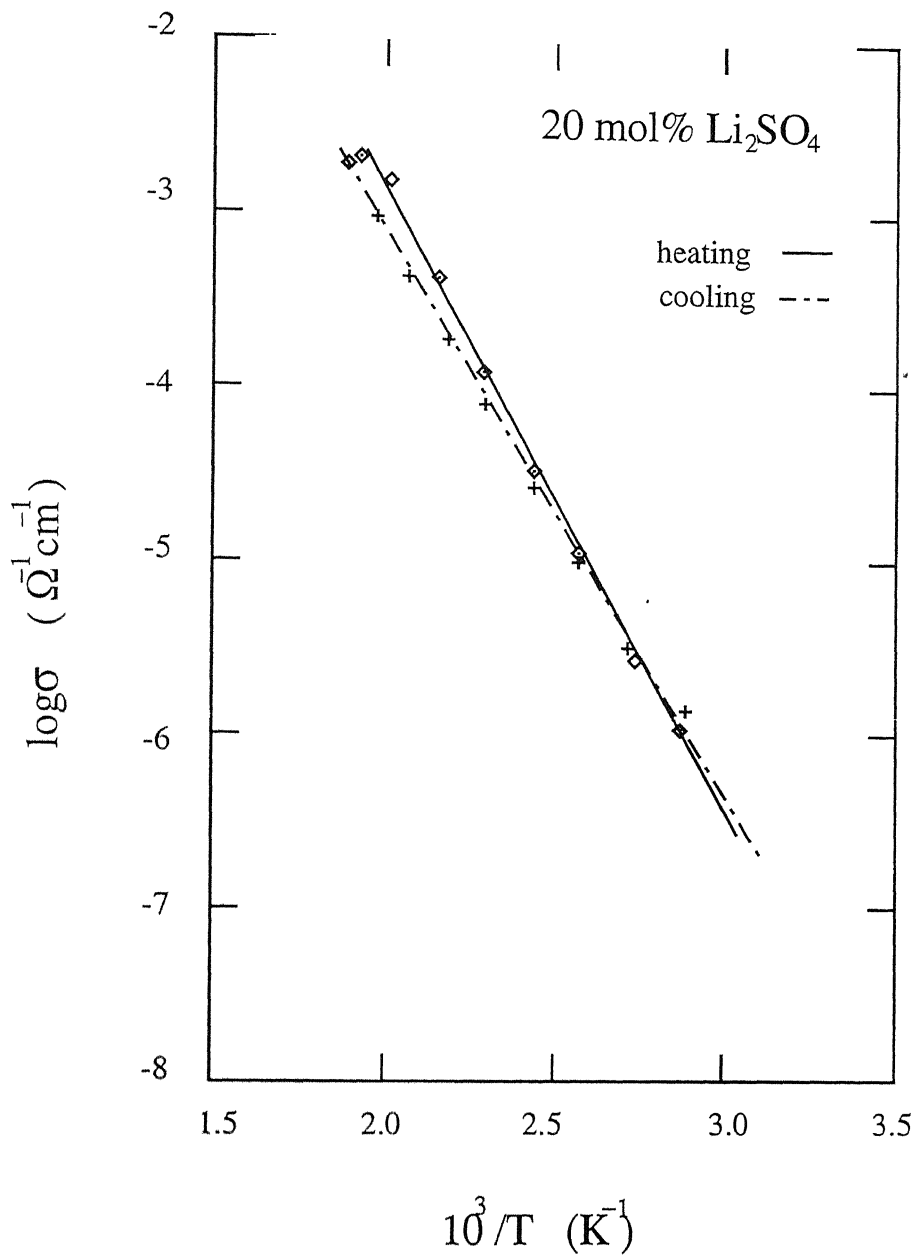


Fig. 3.9: Logarithm of dc conductivity vs. inverse temperature plot for both heating and cooling cycles in the glassy state for S20 sample

To verify the phenomena associated with glass transition and the transition temperature, a crystalline sample of same composition as that of the S20 was prepared and it was found that the conductivity of this crystalline sample was almost exactly

the same as that obtained in the cooling cycle of the glassy material after crossing  $T_g$  i.e., after it gets crystallized. These results are shown in Fig 3.10 .

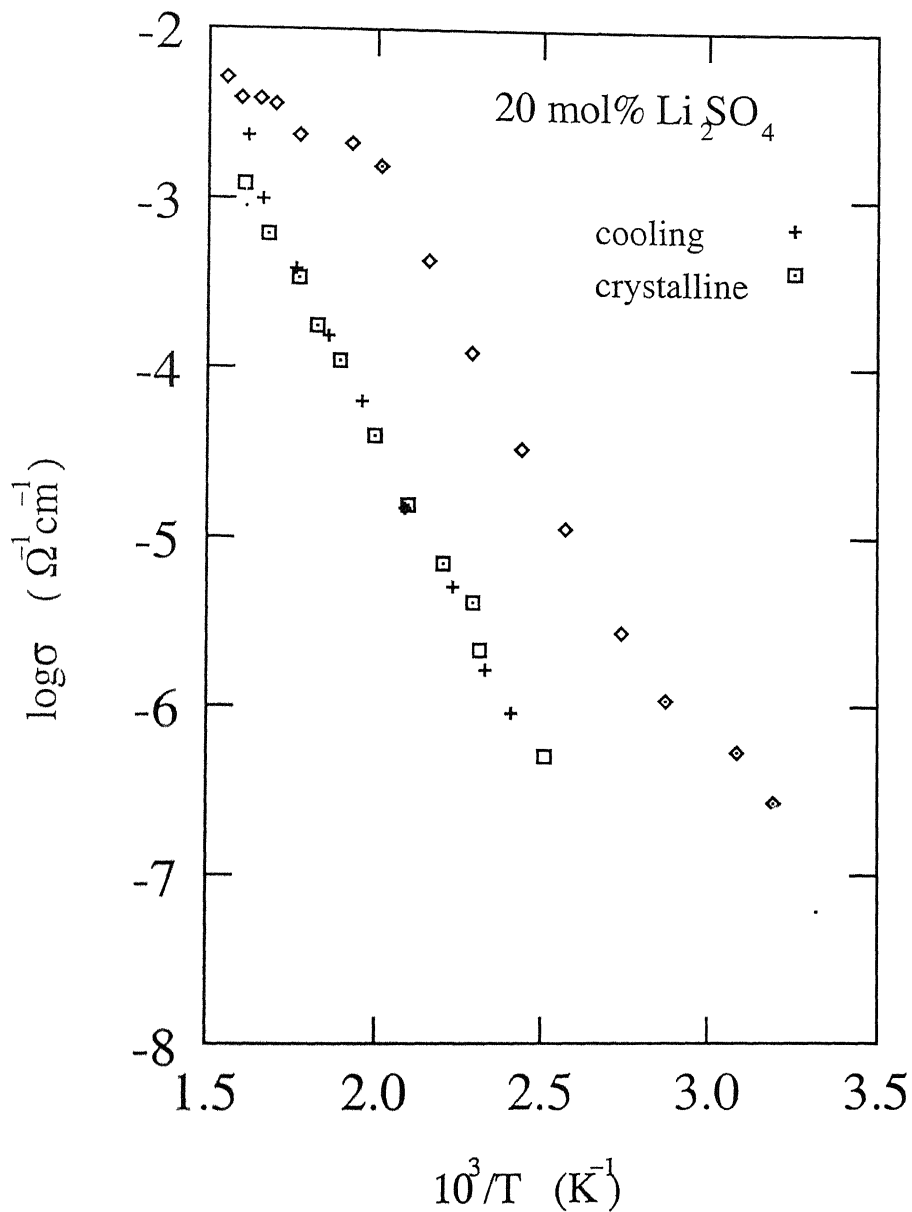


Fig. 3.10: A comparison of electrical conductivity of the S20 glass (in cooling cycle) with that of crystalline mixture of the same composition

### 3.4 Electrical Conductivity Vs. Composition:

It is observed that the electrical conductivity increases with increasing concentration of  $\text{Li}_2\text{SO}_4$  (upto 20 mol %) in the  $\text{Li}_2\text{O} + 25 \text{ mol}\% \text{ B}_2\text{O}_3$  host system.  $\text{Li}_2\text{SO}_4$  may be considered to be a weak electrolyte which gets dissociated in the network without any notable reaction.<sup>[22]</sup> It incorporates mobile  $\text{Li}^+$  ions to the glass matrix, which carry electricity. And the sulphate ions break the oxygen bridges and thereby transform the  $\text{SO}^{-3}$  units into  $\text{BO}^{-4}$  tetrahedra. Therefore lithium sulphate modifies the macromolecular network by increasing the number of NBO present in the glass. Also the network gets stretched because of the large size of sulphate ions.<sup>[15]</sup> The proposed scheme of dissociation of lithium sulphate in the LB glass is

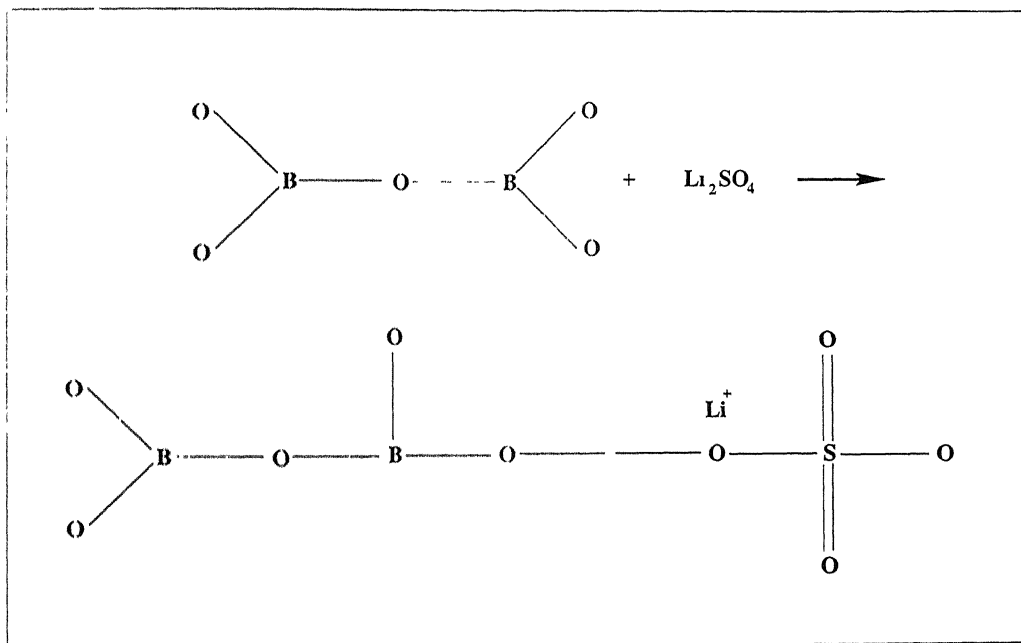


Fig. 3.11: Dissociation mechanism of  $\text{Li}_2\text{SO}_4$  in the LB system

In a statistical mechanical model<sup>[25]</sup> of ionic conductivity, the dissociation reaction has been reported to be



This model supports the above proposed scheme of  $Li_2SO_4$  incorporation in the glass matrix

However further increase in  $Li_2SO_4$  molar percentage i.e., above 20 mol%, causes a decrease in the conductivity. The possible reasons are

(1) For such high ratio of  $Li_2SO_4$ , the  $SO_4^{2-}$  ions do not get dissociated in the LB host system fully. So a part of added dopant salt remains undissolved in the glassy network. They retain their crystalline key structure. And thus ionic mobility becomes less.

(2) It may be possible to form perfect glass for some compositions with high percentage of  $Li_2SO_4$ , but still conductivity may decrease due to “mutual interaction” between the mobile  $Li^+$  ions as density of those ions will be high in that case.<sup>[5]</sup>

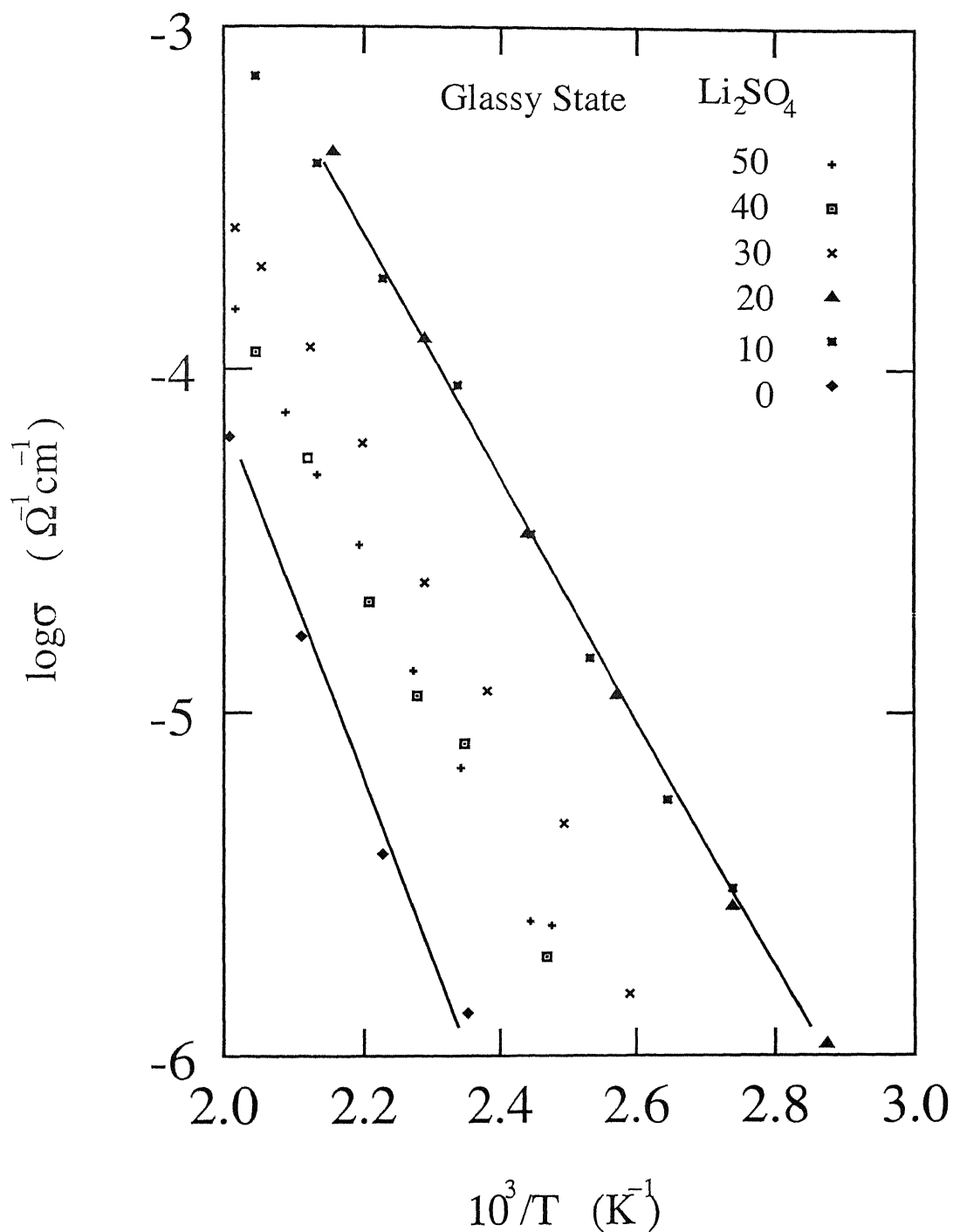


Fig. 3.12: The variation of electrical conductivity as a function of inverse temperature for six different compositions. The samples containing 0, 10 and 20 mol%  $\text{Li}_2\text{SO}_4$  are essentially glassy, while the rest are actually mixture of glass and crystalline materials.

The variation of conductivity as a function of composition, i.e., mol% is shown Fig. 3.13 at two different temperatures (400 and 500 K). Also shown in the Figure is the fraction of  $\text{Li}^+$  ions calculated from the formula

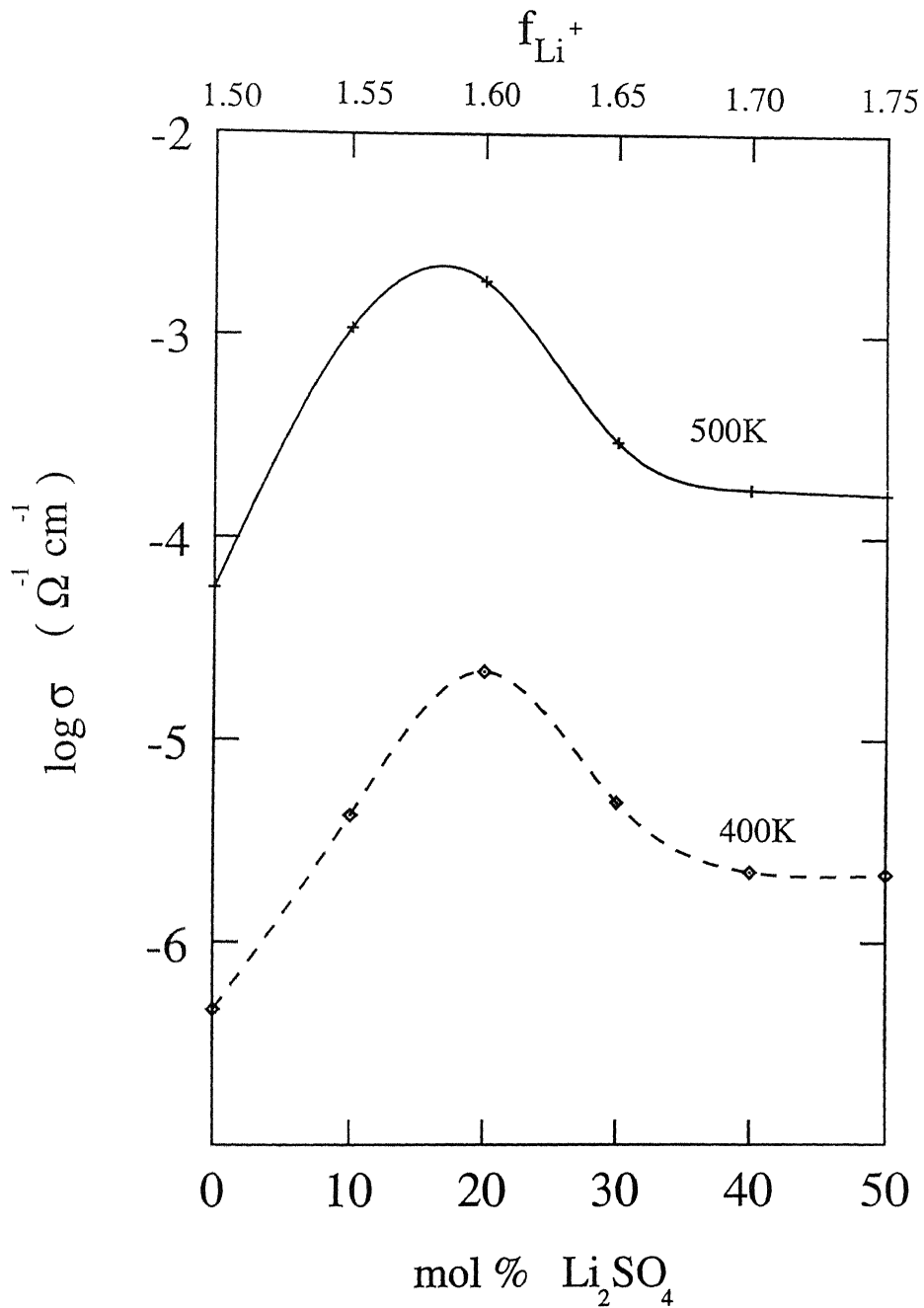


Fig. 3.13: Variation of electrical conductivity with composition at  $T = 400$  &  $500$  K.

$$f_{Li^+} = \frac{2n_{Li_2O} + 2n_{Li_2SO_4}}{n_{Li_2O} + n_{Li_2SO_4} + n_{B_2O_3}} \quad (3.4)$$

It is clearly observed that the sample with 20 mol %  $Li_2SO_4$  has the maximum conductivity (about two order of magnitude higher than the host). This observation fulfills our expectation and supports the view that  $x = 20$  composition as the optimised glass composition (Section 3.1). The conductivity is much less in the partially crystalline samples with higher ratio of  $Li_2SO_4$ .

Fig. 3.14 shows the activation energy vs. mol%  $Li_2SO_4$ . It is of great interest to note that as the conductivity increases with the inclusion of salt in the glassy host, the activation energy decreases to a minimum value of 0.60 eV for the S20 sample which is most conducting. This is as expected.

From Fig. 3.14 it is observed that the activation energy of the host system is 0.82 eV. When lithium sulphate is added by 10 mol% to this host, the energy required for movement decreases. This decrease in activation energy value is maximum for 20 mol%  $Li_2SO_4$  ( $E_a = 0.60$  eV). This is what is expected since addition of more  $Li_2SO_4$  produces large number of NBOs and thus the channels of the glass network becomes more wide. Thus the mobile ions can move freely and energy for transportation (here, migration energy) decreases. And the result is consistent with the conductivity values (Fig. 3.13). Conductivity is the maximum for 20 mol%  $Li_2SO_4$ .

However, activation energy increases when lithium sulphate is added more than 20 mol%. For those compositions, the conductivity decreases keeping sound relationship with increase in activation energy. And it is obvious because inclusion of  $Li_2SO_4$  more than 20 mol% becomes an obstacle for forming perfect glass and thus the material remains partially crystalline.

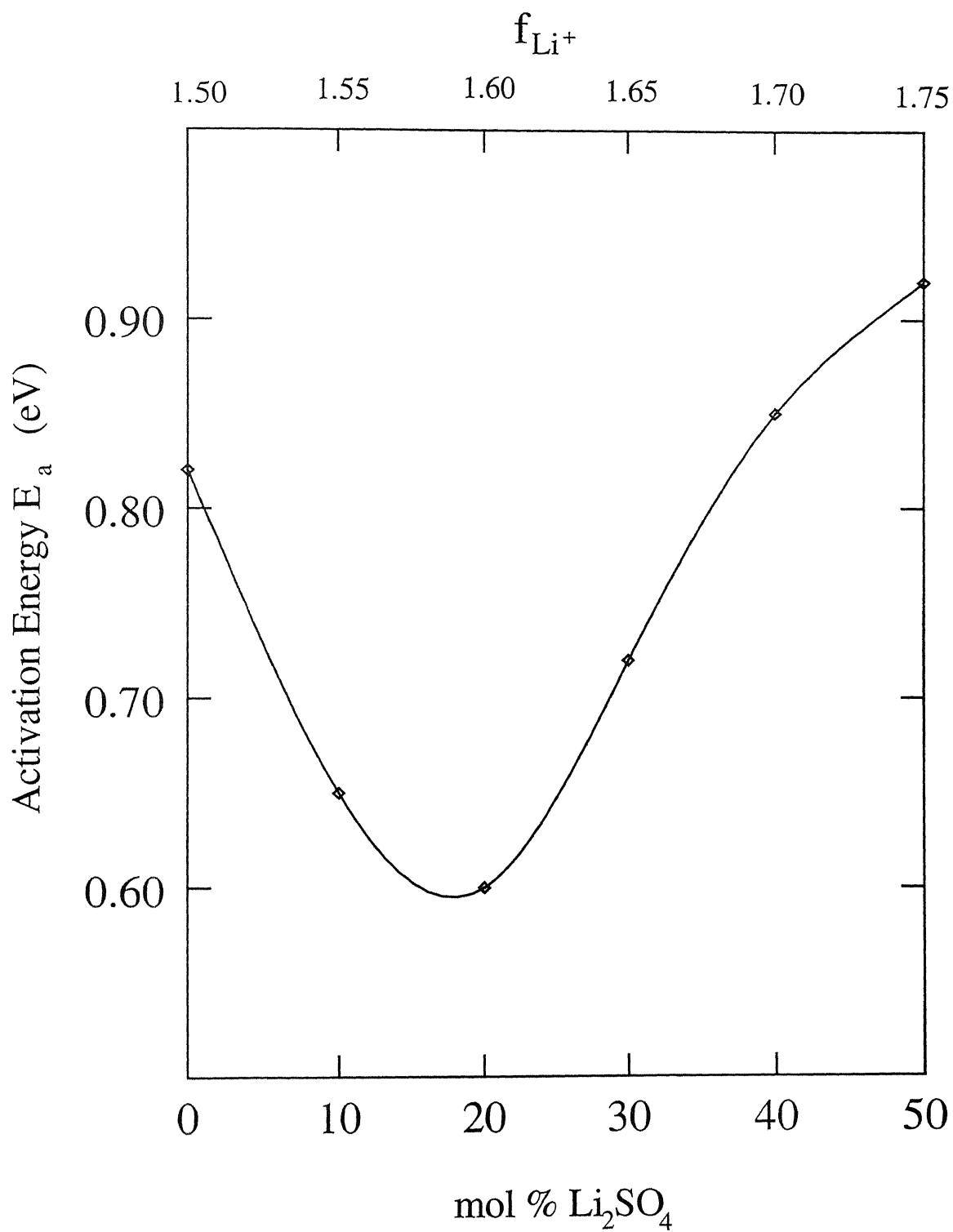


Fig. 3 14. Variation of activation energy  $E_a$  with composition



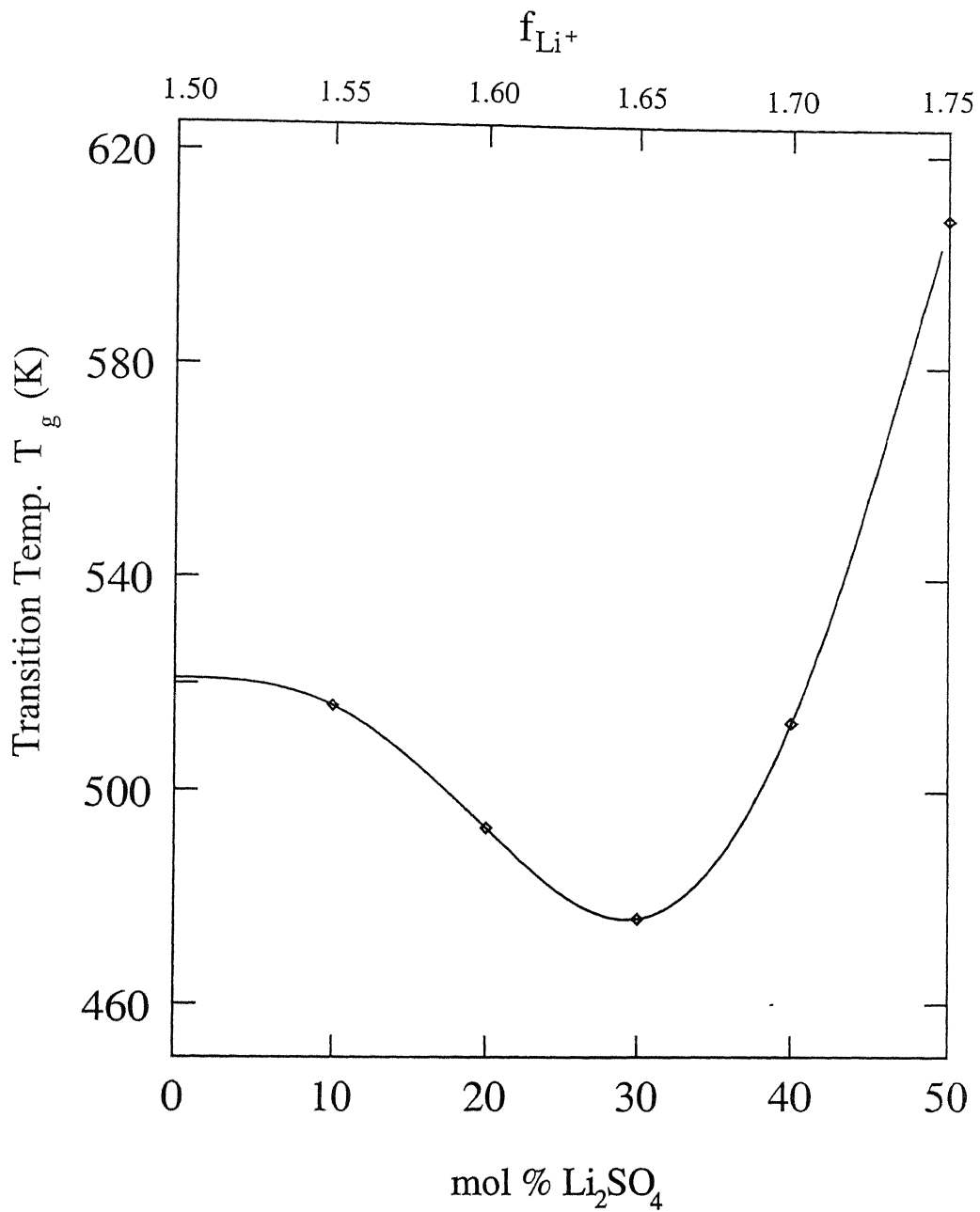


Fig. 3.15: Variation of transition temperature  $T_g$  with composition

The following Table is a summary of the transition temperature, electrical conductivity at 400 and 500 K and the activation energy for various glass samples studied in this work. A maximum conductivity of  $\sim 1.85 \times 10^{-3}$  at 500 K is obtained for the S20 glass, which is orders of magnitude higher than that of pure  $\text{Li}_2\text{SO}_4$

**Table 3.2:** Transition temperature, conductivity and activation energy values for different compositions:

Mol % Li <sub>2</sub> SO <sub>4</sub> x	Transition Temp. T <sub>g</sub> (K)	Conductivity σ (Ω <sup>-1</sup> cm <sup>-1</sup> )				Activation energy E <sub>a</sub> (eV)
		Crystalline		Glassy		
		400 K	500 K	400 K	500 K	
50	608	1.22×10 <sup>-7</sup>	8.10×10 <sup>-6</sup>	2.16×10 <sup>-6</sup>	1.64×10 <sup>-4</sup>	0.92
40	513	1.21×10 <sup>-7</sup>	2.39×10 <sup>-6</sup>	2.24×10 <sup>-6</sup>	1.74×10 <sup>-4</sup>	0.85
30	476	6.54×10 <sup>-7</sup>	4.52×10 <sup>-5</sup>	4.94×10 <sup>-6</sup>	2.97×10 <sup>-4</sup>	0.72
20	493	3.77×10 <sup>-7</sup>	4.38×10 <sup>-5</sup>	2.17×10 <sup>-5</sup>	1.85×10 <sup>-3</sup>	0.60
10	516	4.24×10 <sup>-6</sup>	1.95×10 <sup>-4</sup>	4.24×10 <sup>-6</sup>	1.08×10 <sup>-3</sup>	0.65
0	521	-	-	4.62×10 <sup>-7</sup>	5.64×10 <sup>-5</sup>	0.82

### 3.5 Impedance Vs. Frequency

The variation of impedance with frequency,  $Z(\omega)$ , could also be used to investigate the dielectric constant and loss and thus the various relaxation process operative in the materials, besides the conductivity which has already been discussed (Section 2.2). The complex impedance/admittance  $Z^* = 1/Y^*$  data is usually presented in any of the following forms,

$$Z^* = 1/Y^* = Z' + jZ'' \quad (3.5)$$

$$Y^* = j\omega C_o \epsilon^* \quad (3.6)$$

$$M^* = 1/\epsilon = j\omega C_o Z^* \quad (3.7)$$

where complex permittivity  $\epsilon^* = \epsilon' - j\epsilon''$  and modulus  $M^* = 1/\epsilon^* = M' + jM''$ . Thus from the same measured impedance data, every other impedance parameter can be calculated.

Fig. 3.16(a)-(c) show the variation of imaginary parts ( $Z'' = Z \sin \theta$ ) of the impedance as a function of frequency at various different temperatures. It is observed that in each case the curve exhibits a sharp maximum at a certain frequency that is characteristic of a relaxation process or mechanism.

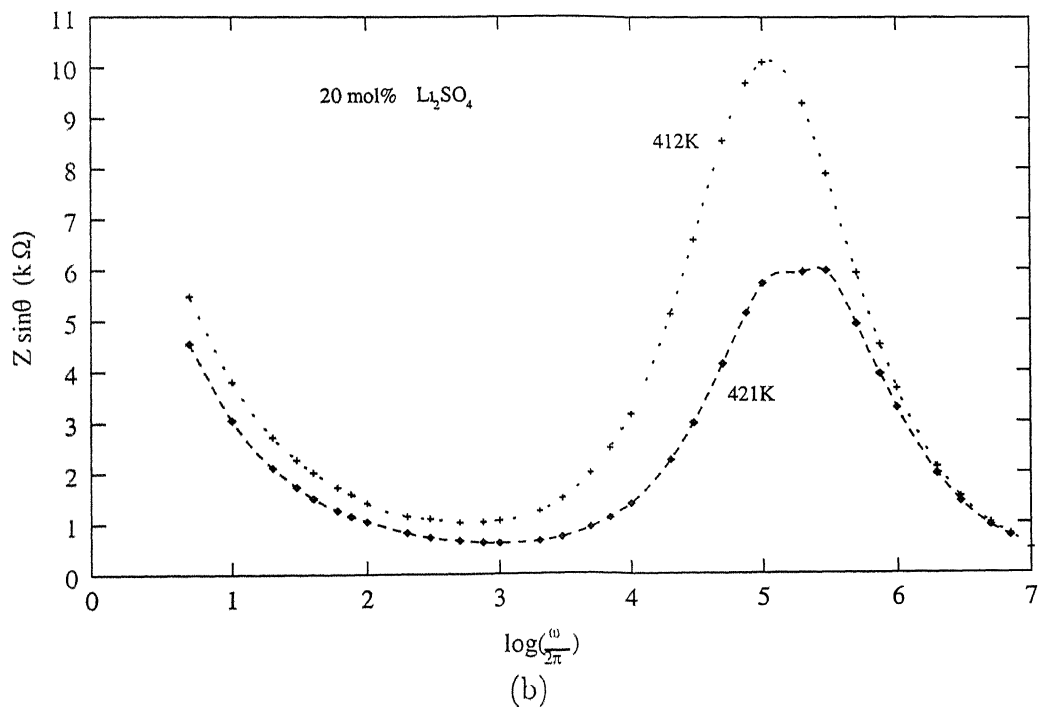
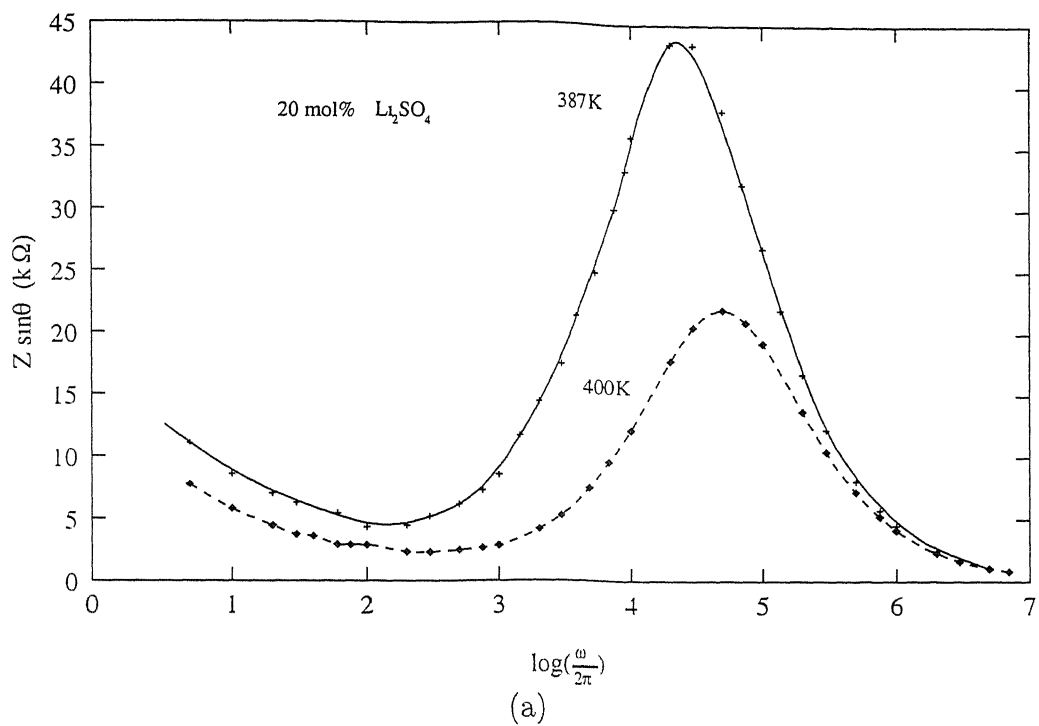


Fig. 3.16(a)-(b): Frequency dependence of the imaginary part ( $Z''$ ) of the complex impedance at 378, 400, 412 and 421 K for S20 glass.

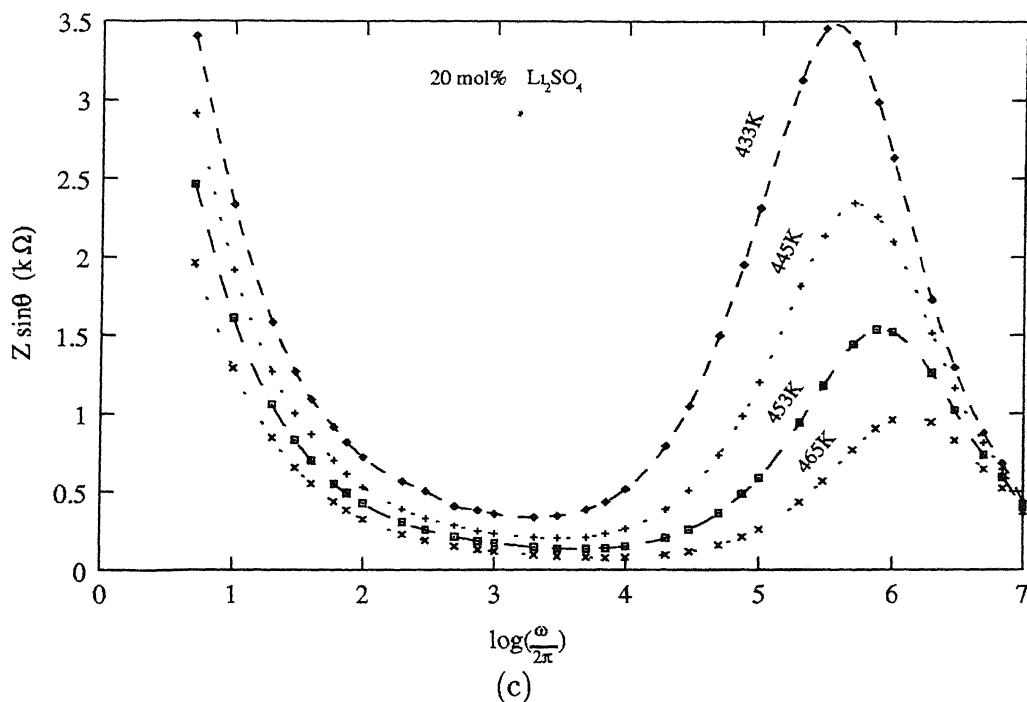


Fig. 3.16(c): Frequency dependence of the imaginary part ( $Z''$ ) of the complex impedance at 433, 445, 453, 465 K for S20 glass.

For any thermally activated process (involving energy  $E_a$ ), the relaxation frequency  $\omega_r$  and full width at half maximum (FWHM)  $\Delta\omega$  are given by

$$\omega_r = \omega_o \exp\left(-\frac{E_a}{kT}\right) \quad (3.8)$$

$$\Delta\omega = \frac{2}{\sqrt{3}}\omega_r \quad (3.9)$$

where  $\omega_o$  is a constant. For such processes, a plot of  $\log\omega$  vs.  $1/T$  plot is linear whose slope yields the activation energy for the associated process. The results shown in Figs. 3.16(a)-(c) do reveal that the peak (relaxation frequency) shifts (increases) as temperature increases, and in fact a plot of  $\log\omega_r$  vs.  $10^3/T$  is linear (Fig. 3.17). The activation energy (1.00 eV) obtained from the slope is however slightly higher than that (0.82 eV) for dc conductivity which may suggest that some processes such as interfacial or dipolar polarization are also involved besides the conduction mechanism.

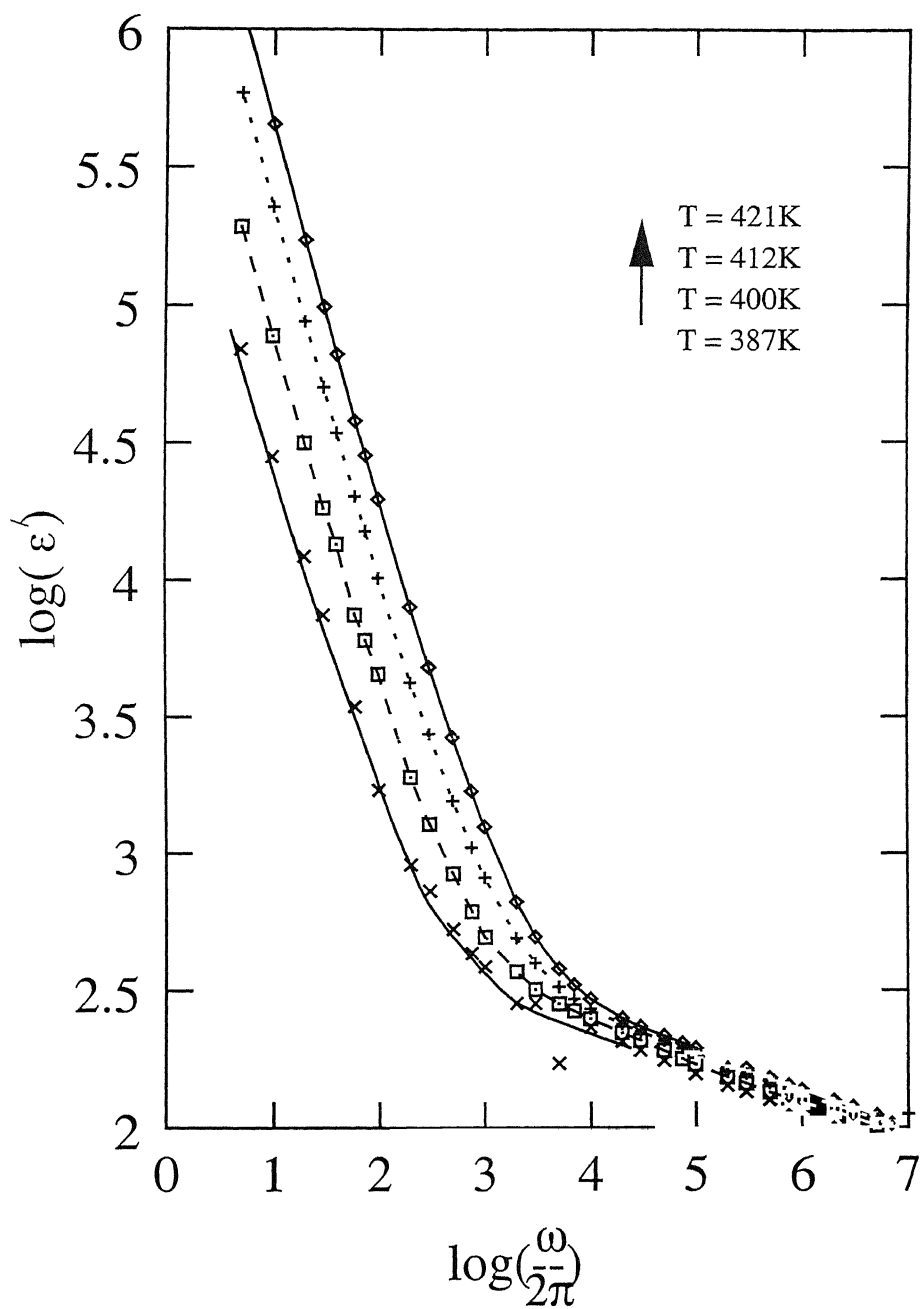


Fig 3.18: The dielectric constant as a function of frequency for the glass S20 at different temperatures.

### 3.5.2 Dielectric Loss:

The dielectric loss ( $\tan\delta$ ) defined as

$$\tan\delta = \frac{\epsilon''}{\epsilon'} \quad (3.10)$$

has also been studied for the same S20 glass. These results are shown in Figs. 3.19.

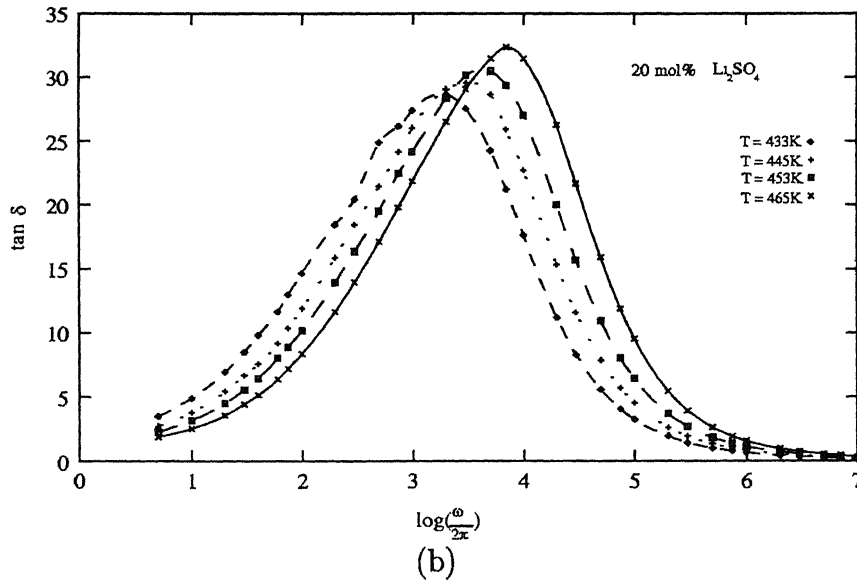
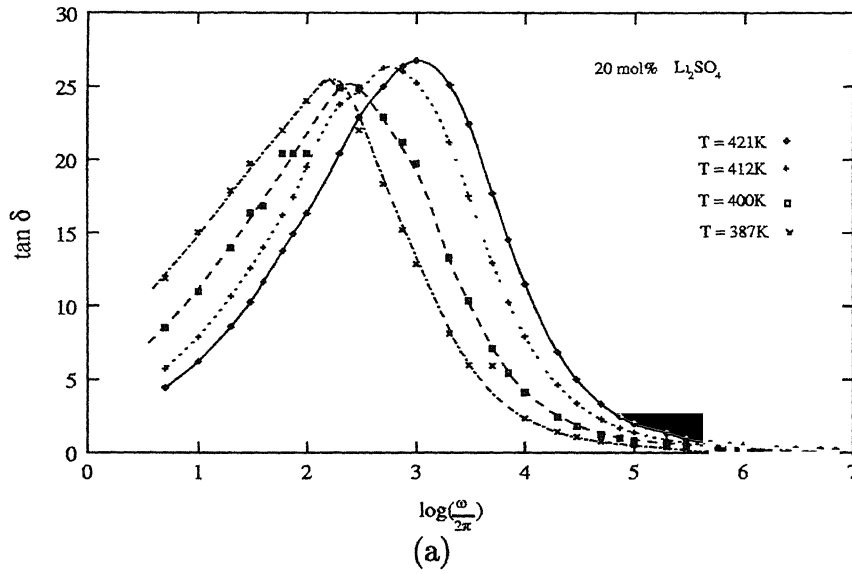


Fig. 3.19(a)-(b): Dielectric loss ( $\tan\delta = \epsilon''/\epsilon'$ ) vs. frequency plot for S20 glass.

Since these glasses are quite conducting a relatively high value of dielectric loss is, however, not surprising. Thus the Li-based glasses investigated in this work may be characterized as highly conducting, polarizable and lossy materials.

The relaxation frequency  $\omega_r$  and the band width (FWHM)  $\Delta\omega$  have been calculated for  $x = 0$  and  $x = 20$  compositions from the  $\tan\delta$ - $\log\omega_r$  curves. The values have been tabulated in table below

**Table 3.3:** The values of the relaxation frequency  $\omega_r$  and FWHM  $\Delta\omega$  extracted from various processes:

Host · x = 0				
Temperature (K)	$\omega_r^{Z''}$	$\Delta\omega^{Z''}$	$\Delta\omega^{\tan\delta}$	$\omega_r^{\tan\delta}$
425	11.7 k	53.7 k	-	-
449	30.2 k	190.5 k	55 Hz	468 Hz
474	154.9 k	707.9 k	372 Hz	1.8 k
498	724.4 k	32.4 M	1.3 k	8.9 k
524	1.2 M	63.1 M	3.1 kHz	18.6 k
20 mol% Li <sub>2</sub> SO <sub>4</sub>				
387	21.4 k	138.0 k	180 Hz	1.1 k
400	46.8 k	251.2 k	251 Hz	2.1 k
412	109.6 k	631.0 k	513 Hz	3.4 k
421	166.0 k	933.3 k	1.1 k	8.1 k
433	346.7 k	1.9 M	1.5 k	14.1 k
445	501.2 k	2.9 M	2.9 k	20.9 k
453	724.4 k	4.6 M	3.9 k	30.2 k
465	1.2 M	7.2 M	6.8 k	47.9 k



### 3.5.2 Activation Energy Revisited:

The  $\log(\frac{\omega_r}{2\pi})$  vs.  $\frac{10^3}{T}$  plots have been shown for  $x = 20$  composition. It gives a straight line, the slope gives the activation energy in a similar way done in section 3.5.

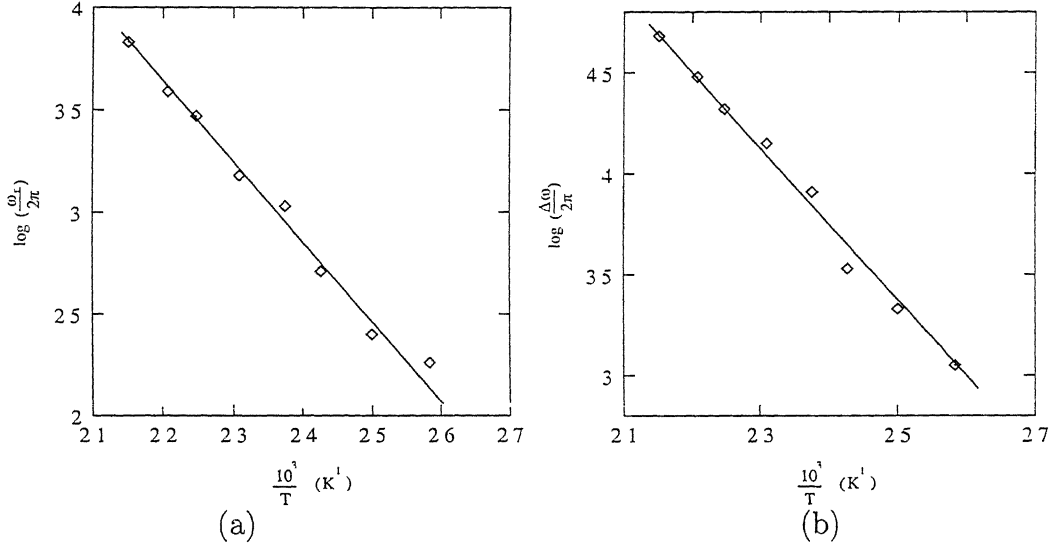


Fig. 3.20: (a)  $\text{Log}(\frac{\omega_r}{2\pi})$  vs.  $\frac{10^3}{T}$  (b)  $\text{Log}(\frac{\Delta\omega}{2\pi})$  vs.  $\frac{10^3}{T}$  plots obtained from dielectric loss for  $x = 20$  composition.

The values of activation energy calculated here matches with those obtained from the section 3.5. All the values obtained from different processes for  $x = 0$  and  $x = 20$  compositions have been shown in the table below.

**Table 3.4:** Activation energy values extracted from various processes:

Composition x	Activation energy $E_a$ (eV)				
	$\sigma_{dc}(T)$	$\omega_r^{Z''}(T)$	$\Delta\omega^{Z''}(T)$	$\Delta\omega^{tan\delta}(T)$	$\omega_r^{tan\delta}(T)$
0	0.82	1.00	0.94	1.09	1.05
20	0.60	0.80	0.94	0.78	0.75

\* The activation energy values for other compositions extracted from  $\sigma_{dc}$  calculation have already been tabulated Table 3.2

# Chapter 4

## Conclusions

[Li<sub>2</sub>O + 25 m/o B<sub>2</sub>O<sub>3</sub>] + x mol% Li<sub>2</sub>SO<sub>4</sub> system in the composition range  $0 \leq x \leq 50$  has been investigated. The quenched sample containing upto 20 mol% Li<sub>2</sub>SO<sub>4</sub> are found to be essentially glassy in nature, while others ( $x > 20$  m/o) are composites of glass and crystalline particles.

The glass transition temperature ( $T_g$ ) is found to decrease with increasing concentration of Li<sub>2</sub>SO<sub>4</sub> upto  $\sim 20$ -30 mol% Li<sub>2</sub>SO<sub>4</sub>, and therefore it begins to increase. Interestingly, the electrical conductivity vs. composition curve follows more or less a similar trend but in opposite sense the conductivity increases as salt concentration increases upto  $\sim 20$  m/o Li<sub>2</sub>SO<sub>4</sub>, while the activation energy decreases and assumes a minimum value of  $\sim 0.60$  eV at about 20 m/o Li<sub>2</sub>SO<sub>4</sub>.

The Li<sub>2</sub>O-B<sub>2</sub>O<sub>3</sub>-Li<sub>2</sub>SO<sub>4</sub> system can be stabilized into highly ionically conducting, has exceptionally high value of dielectric constant and moderately high value of dielectric loss. For example, the S20 glass (containing 20 mol% Li<sub>2</sub>SO<sub>4</sub>) has a  $\sigma \sim 10^{-3}$  ohm<sup>-1</sup> cm<sup>-1</sup>,  $\epsilon' \sim 10^6$  and  $\tan\delta \approx 25$  at 1 kHz. Thus these glassy fast ion conductors have potential for use in cells/batteries, supercapacitors and other electrochemical devices.

The present preliminary work also suggests that there is a wide range of compositions and choice of materials that should be further explored to optimize the properties

## REFERENCES

- 1 Hooper A. *Contempt. Phys.* **19** (2), 1978, 147-168.
- 2 Deshpande V. K , Raghuwanshi F. C., Singh K. *Solid State Ionics* **18-19**, 1986, 378-381.
3. Deshpande V K , *Solid State Ionics* **40-41**, 1990, 689-192
- 4 Li-quan C , Lian-zhong W , Guang-can C., Gang W., Zi-rong L., *Solid State Ionics* **14**, 1984, 149-152
- 5 Rokade R , Singh K., Deshpande V. K., *Solid State Ionics* **18-19**, 1986, 374-377.
6. Barasoum M. W., Tuller H. L., *Solid State Ionics* **18-19**, 1986, 388-392.
7. Ravaine D., *J. Non-Crystalline Solids* **38-39**, 1980, 353-358.
8. Soppe W., Marel C. V D., Hartog H. W. D., *J. Non-Crystalline Solids* **101**, 1988, 101-110.
9. Irion M., Couzi M., *J. Solid State Chem.* **31**, 1980, 285-294.
10. Krogh-Moe J., *Phys Chem. Glasses* **6**, 1966, 46.
11. Jullen C., Massot M., *Solid State Ionics* **34**, 1989, 269-173.
12. Kamitsos E. I., Karakassides M. A., Chryssikos G.D., *Phys. Chem. Glasses* **28** (5), 1987, 203-209.
13. Smedley S., I., Angell C A., *Solid State Comm.* **27**, 1978, 21-23.
14. Otto K., *Phys. Chem. Glasses* **7** (1), 1966, 29-37.
15. Gandhi P. R , Deshpande V. K., Singh K., *Solid State Ionics* **36**, 1989, 97-102.
16. Xihuai H., Pengnian H., *J. Non-Crystalline Solids* **80**, 1986, 435-439

17. Ayyadi A., Massot M., Balkanski M., *Physica Scripta*. **38**, 1988, 75-77.
18. Button D. P., Tandon R., King C., Velez M. H., Tuller H. L., Uhlmann D. R.,  
*J. Non-Crystalline Solids* **49**, 1982, 129-142.
19. Glass A. M., Nassau K., Negran T. J., *J. Appl. Phys.* **49** (9), 1978, 4808-4811.
20. Kamitsos E. I., Karakassides M. A., Chrysikos G. D., *J. Phys. Chem.* **91**,  
1987, 5807-5813.
21. Kamitsos E. I., Karakassides M. A., Chrysikos G. D., *J. Phys. Chem.* **90**,  
1986, 4528-4533.
22. Balanski M., Ayyadi A., Cadet P., Jouanne M., Jullien C., Massot M., Scagliotti M., *Solid State Comm.* **57** (1), 1986, 41-46.
23. Sujata C., *Fast Ion Transport in Lithium Based Solid Electrolytes PhD Thesis*  
(IIT Kanpur), 1992, 90-95.
24. Julien C., Nazri G. A., *Solid State Batteries: Materials Design and Optimization* **Kluwer Academic Publishers**, 1994, 183-195.
25. Balanski M., Wallis R. F., Darianoian I., Deepe J., *Mats. Sc. Engg. B1* **15**,  
1988.